



Cite this: *J. Mater. Chem. A*, 2024, **12**, 14186

## Prospects of polymer coatings for all solid-state and emerging Li-ion batteries†

Ruhul Amin, <sup>‡\*</sup><sup>a</sup> Umair Nisar, <sup>‡\*</sup><sup>b</sup> Muhammad Mominur Rahman, <sup>a</sup> Marm Dixit, <sup>a</sup> Ali Abouimrane <sup>a</sup> and Ilias Belharouak <sup>\*</sup><sup>a</sup>

Polymers possess processing flexibility as they can be coated on cathode particles before/after electrode fabrication and on the solid-state electrolyte surface in all-solid-state batteries (ASSBs). Their narrow electrochemical stability window limits the use of polymers directly as an electrolyte against high voltage cathodes. However, when a polymer is coated directly on battery cathodes and cycled with conventional liquid electrolytes, they exhibit superior battery performance in comparison to uncoated ones. A deeper insight was not sought in the literature. There might be a great possibility of *in situ* formation of an ultra-thin protective layer in-between the polymer and cathode interface at the coating development stage or in the formation cycle of the electrochemical cell. The current ASSBs demand flexible, easily scalable coating materials, which can accommodate the volume expansion–contraction during cycling and can minimize the lattice stress. However, a much better fundamental understanding is needed on polymer/ceramic interfaces. This focused review is concentrated on flexible polymers with high ionic and electronic conductivities that can be used for coating cathode particles and Li anodes. Overall, this article has analyzed and validated the application of various types of polymers in lithium-ion batteries

Received 15th February 2024  
Accepted 7th May 2024

DOI: 10.1039/d4ta01061b  
[rsc.li/materials-a](http://rsc.li/materials-a)

<sup>a</sup>Electrification and Energy Infrastructures Division, Oak Ridge National Laboratory, Oak Ridge, TN 37831, USA. E-mail: [aminr@ornl.gov](mailto:aminr@ornl.gov); [belharouak@ornl.gov](mailto:belharouak@ornl.gov)

<sup>b</sup>Centre for Solar Energy and Hydrogen Research Baden-Württemberg (ZSW), Helmholtzstraße 8, 89081 Ulm, Germany

† This manuscript has been co-authored by UT-Battelle, LLC, under contract DE-AC05-00OR22725 with the US Department of Energy (DOE). The US government retains and the publisher, by accepting the article for publication, acknowledges that the US government retains a nonexclusive,

paid-up, irrevocable, worldwide license to publish or reproduce the published form of this manuscript, or allow others to do so, for US government purposes. DOE will provide public access to these results of federally sponsored research in accordance with the DOE Public Access Plan (<http://energy.gov/downloads/doe-public-access-plan>).

‡ These authors contributed equally.



Ruhul Amin

Dr Ruhul Amin is a Senior R&D Staff Scientist at the Oak Ridge National Laboratory. He received his bachelor's and master's degrees in chemistry from Dhaka University, Bangladesh, and his doctoral degree in materials science and engineering from Max Planck Institute, Stuttgart, Germany. Dr Amin worked at various prestigious institutes including the Massachusetts Institute of Technology (MIT). His major

research thrust is in energy storage and conversion. Dr Amin received several awards including an R&D 100 award. He has published more than 115 papers, 6 book chapters and 15 US patents and patent applications in the field of electrochemical energy storage and conversion.



Umair Nisar

Umair Nisar is currently pursuing his PhD in Chemistry at the Center for Solar Energy and Hydrogen Research Baden-Württemberg (ZSW) in Germany. He got his master's degree in Materials Science & Engineering from the Korea Advanced Institute of Science & Technology (KAIST) in South Korea and his Bachelor's degree from the GIK Institute of Engineering Sciences and Technology (GIKI) in Pakistan. Umair has previously worked as a research engineer at POSCO Energy Storage Materials (POSCO ESM) in South Korea, developing high-Ni layered oxide cathode materials. His current research focuses on developing high-voltage spinel  $\text{LiNi}_{0.5}\text{Mn}_{1.5}\text{O}_4$  cathode materials for next-generation lithium-ion batteries.



and ASSBs comprehensively with an emphasis on the effect of coating morphologies and thickness on performance. Finally, this review gives a brief discussion on the prospects and suitability of polymers as coating layers.

## 1. Introduction

At present, the global energy sector is experiencing a transition from conventional energy sources to the zero-emission renewable field. Energy storage systems play a vital role in accelerating the implementation of this transition. The fast-growing market of rechargeable lithium-ion batteries (LIBs) for electric vehicles (EVs), electric vertical takeoff and landing (eVTOL), outer space applications, and renewable energy sources demands the development of advanced batteries that are extremely safe, cost-

effective, and have a high energy and power density.<sup>1–3</sup> LIBs have high energy and power density and control the market of both portable electronics and electric vehicles. Currently, the major focus is concentrated on the electrification of transportation and the development of large energy storage systems (ESSs) for efficient use of renewable sources.<sup>4–9</sup> Unfortunately, the current conventional liquid-based lithium-ion batteries still suffer from poor safety, lower cycle life, low energy, and low power density, which have seriously affected their widespread acceptance in EVs and eVTOL.<sup>10–12</sup> However, all-solid-state lithium metal batteries (ASSLMBs) are a promising alternative to traditional



**Muhammad Mominur Rahman**

National Laboratory (July 2021–December 2023) under the DOE Battery500 consortium. His current research interest lies in materials development and characterization of batteries beyond Li-ion batteries and batteries for electric vertical take-off and landing (eVTOL) platforms.

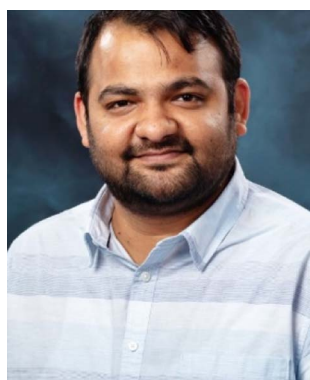
*Muhammad Mominur Rahman is a Weinberg Distinguished Staff Fellow at the Oak Ridge National Laboratory. He received his PhD in Chemistry (2021) from Virginia Tech. For his graduate research work in Na-ion batteries, he was awarded the Electrochemical Society Battery Division student research award in 2021. Before joining ORNL, he worked as a postdoctoral research associate at the Brookhaven*



**Ali Abouimrane**

than 80 peer-reviewed journal papers, 15 granted patents and around 15 patent applications in the areas of Energy Storage. Dr Abouimrane received numerous awards, including the best NRC-Canada employee award and R&D 100 award.

*Dr Ali Abouimrane is a Senior Scientist at ORNL with over 24 years' experience in rechargeable batteries and materials. Before joining ORNL, Dr Ali Abouimrane was Sparkz Inc. VP of Technology from 2021 to 2022. From 2015 to 2020, Dr Abouimrane was a Principal Scientist at Qatar Foundation and from 2008 to 2015 a Materials Scientist at the Argonne National Laboratory. Dr Ali Abouimrane published more*



**Marm Dixit**

awarded the ECS Toyota Young Investigator Fellowship 2021, APS Rosalind Franklin Young Investigator Award in 2023, and was a finalist for the 2024 ACS Energy Lectureship. He has published more than 45 papers in the field of electrochemical energy storage and conversion.

*Dr Marm B. Dixit is a R&D Staff Scientist and an ex-Weinberg Distinguished Staff Fellow at the Oak Ridge National Laboratory. Marm received his bachelor's degree in mechanical engineering from the Charotar University of Science and Technology, India, and his doctoral degree from Vanderbilt University. His doctoral thesis was on understanding processing-structure-function relationships in solid electrolytes. Marm was*



**Ilias Belharouak**

awards and four U.S. Federal Laboratory Consortium Awards. Dr Belharouak is an author of more than 190 peer-reviewed papers, 50 US patents and patent applications, and 5 books. Dr Belharouak is the Editor of the *Journal of Power Sources*.

*Dr Ilias Belharouak is a Corporate Fellow and Head of the Electrification Section at the Oak Ridge National Laboratory and Professor at the Bredesen Center for Interdisciplinary Research and Graduate Education of the University of Tennessee Knoxville. He is an advisory board member for several US universities and government agencies. Dr Belharouak has received numerous awards, including six R&D 100*



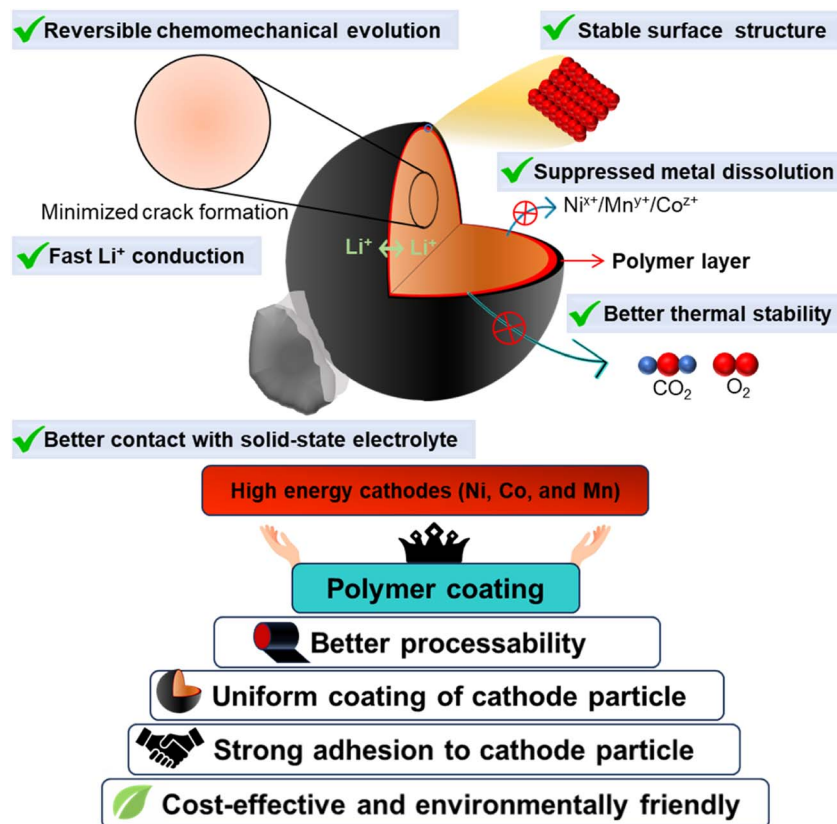


Fig. 1 Schematic demonstration of the benefits and role of polymer-based surface coatings in high performance lithium-ion battery cathodes.

liquid-based lithium-ion batteries because of their safety and higher energy density. The significant benefit of ASSLMBs comes from the extremely high theoretical capacity of lithium metal anodes ( $3860 \text{ mA h g}^{-1}$ ), low density ( $0.53 \text{ g cm}^{-3}$ ), and the lowest reduction potential ( $-3.04 \text{ V}$  vs. the standard hydrogen electrode) among metals. Furthermore, the low probability of leakage and vaporization of inorganic solid-state electrolytes (SEs) provides safe operational assurance.<sup>13,14</sup> Note that SEs largely determine the overall performance of ASSLMBs.<sup>15,16</sup> There are mainly two broad groups of solid electrolytes: (a) inorganic solid-state electrolytes (*e.g.*, oxide and sulfide) and (b) polymer based. Every group of SEs has its inherent advantages and disadvantages, and detailed discussion is out of the scope of this review article. The oxide-based SEs are relatively stable against cathode and Li metal anode interfaces. However, they exhibit poor contact formation and low ionic conductivity, resulting in higher impedance and cell polarization at ambient temperature. On the other hand, sulfide-type solid electrolytes (SSEs) are highly attractive due to their high ionic conductivity ( $>1 \text{ mS cm}^{-1}$  at room temperature) and excellent processibility in terms of their mechanical stiffness. SSEs can form an intimate contact with electrode materials.<sup>17,18</sup> Unfortunately, SSEs have been reported to be less compatible with the Li anode as well as high voltage cathodes, which results in an ever-increasing interfacial resistance and narrow operational voltage window.<sup>19</sup> Usually, SSEs slowly go through a spontaneous reduction reaction through consuming

the lithium ions and electrons from the metallic lithium anode and lead to a large interfacial resistance at Li/SSEs. To tackle these challenges of electrode/electrolyte interfacial stability and formation of a robust interfacial contact, many strategies have been formulated as demonstrated in Fig. 1 and given as follows:

- Formation of a protective layer on the Li anode using different coating materials, such as  $\text{LiH}_2\text{PO}_4$  and  $\text{Al}_2\text{O}_3$ , that can passivate the Li anode and suppress the parasitic reactions and Li dendrite growth at the interface.<sup>20</sup>

- Assimilation of ionic liquids (ILs) such as LiTFSI/PYR13TFSI at electrode/electrolyte interfaces is beneficial to improve the interfacial compatibility across Li anode/SEs and cathode/SEs.<sup>21</sup>

- Incorporation of a double-layer configuration of two different SEs compatible with individual electrodes. For example, when LGPS/LSPCL as a double-layer SE is assembled into ASSLMBs, the Li metal compatibility of LSPCL acts as a buffer layer to reduce the reductive decomposition of LGPS electrolyte.<sup>21</sup>

Although the approaches and techniques mentioned above can ameliorate the interface compatibility to a certain extent, easily scalable interfacial coating, minimization of interfacial impedance, and sacrificed energy density of full cells cannot be ignored. A polymer coating on Li anode and cathode particles has significant advantages over oxide-based coatings. A large number of articles have been published on polymer-based coatings using various types of polymer materials and their



electrochemical performances have been discussed and compared with that of uncoated electrode materials. However, several review articles were published on oxide coatings and the polymer coating of electrodes was overlooked. The reported electrochemical performance of polymer-coated electrodes differs significantly in published studies. This might be due to the variation of coating morphology and thickness, intrinsic ionic and electronic conductivities, and mechanical properties of different polymer materials. Note that the paradigm-shifting current all-solid-state batteries demand flexible and easily scalable coating materials with high ionic/electronic conductivity that can accommodate the volume expansion–contraction during charging/discharging. In addition, hybrid electrolytes (polymer/oxide or sulfide electrolytes) may provide a solution to the challenges ASSBs are facing currently. However, for the informed development of polymer and hybrid polymer electrolytes for ASSBs, a much better fundamental understanding is needed about polymer/ceramic interfaces. Here, the focus is concentrated on flexible polymers with high ionic and electronic conductivities that are used for coating on cathode particles and Li anodes and their advantages. Also, this comprehensive review article critically analyzes and validates the application of various types of polymer materials in ASSBs and discusses the prospects of polymers as coating layers in all-solid-state batteries.

## 2. Purpose of cathode surface coating

Since the commercialization of LIBs in 1991 by Sony, their performance in terms of cycle life, energy and power density, and safety kept increasing and the price is gradually decreasing. With the penetration of lithium-ion batteries in electric vehicle applications, the demand and performance of these battery systems also increased. The typical cathodes in LIBs such as high-Ni  $\text{LiNi}_{1-x-y}\text{Mn}_x\text{Co}_y\text{O}_2$  (NCM, Ni > 60%) and  $\text{LiNi}_{0.8}\text{Co}_{0.15}\text{Al}_{0.05}\text{O}_2$  (NCA) are very reactive and unstable during battery operations, especially at higher cut-off voltages and higher operating temperatures. The instability issues arise from the reactivity of organic liquid electrolytes leading to their decomposition in the presence of these cathodes. This not only affects the battery performance but also raises serious safety concerns. On the other hand, in an all-solid-state battery (ASSB), the cathode's active particles must establish a robust ionic conducting network to facilitate rapid charging and discharging of the battery. Therefore, to effectively utilize these cathodes in organic electrolyte systems and in ASSBs, the cathode/electrolyte interface should be stabilized. The coating of cathode particles is one of the ways to achieve interface stabilization. Currently, metal oxides such as  $\text{Al}_2\text{O}_3$ ,  $\text{ZrO}_2$ , and  $\text{SiO}_2$  are extensively used as coating materials due to their high chemical stability predominantly with liquid electrolytes.<sup>22–26</sup> However, more recently, polymer-based cathode coatings have also seen rising interest in the research community. These coatings can not only act as a physical barrier between the cathode surface and the electrolyte but also act as an artificial

cathode–electrolyte interface (CEI) if properly tuned and function as an ion-conducting pathway for ASSBs. A polymer-based cathode coating can have better electronic and ionic conductivities when compared to ceramic-based coatings. Moreover, the processing of polymer coatings is expected to be more viable and can accommodate the volume expansion–contraction under operation compared to oxide coating materials. The main role and functionality of an ideal surface coating are listed below,

- A physical barrier between the cathode and electrolyte: the coating acts as a physical barrier between the cathode and the electrolyte, which reduces any unwanted parasitic reactions between them, especially during higher voltage and high temperature operations. Therefore, the coatings can increase the chemical and electrochemical stability of cathodes when in direct contact with the electrolyte.

- HF scavenger: the coatings can act as an HF (hydrofluoric acid) scavenger in the organic electrolyte system to prevent the degradation of cathode materials. These coatings behave as sacrificial materials, which react with the HF themselves and protect the cathode materials to enhance their long-term cycling stability.

- Improve charge transfer: the ideal surface coating should improve the contact and reduce the charge transfer impedance and enhance the kinetics at the cathode/electrolyte interface. This can be achieved by utilizing ionically and electronically conducting materials. For instance, the poor electronic conductivity of  $\text{LiFePO}_4$  is improved by carbon coating, which concurrently enhances the electron transfer at the interface. The simultaneous ionic and electronically conducting polymers often function better than carbon coatings.

- Stabilization of active particles: the surface coatings should have the ability to suppress the impact of volume expansion–contraction of cathode materials during long-term cycling. This can mitigate the cyclic stress and thus also prevent cracking of cathode particles. Polymer coating materials can more effectively accommodate the volume change than oxide materials. Moreover, coatings on cathode particles can prevent a phase transformation and improve the stability of the material. All these can effectively reduce particle crack formation and prevent the exposure of fresh cathode surface to the electrolyte. Such stabilization is beneficial for reducing transition metal dissolution from the cathode to the electrolyte.

To summarize, a polymer-based surface coating should ideally be conformal, acting as a physical barrier between cathode active particles and the electrolyte. This barrier serves as an artificial interphase at the cathode/electrolyte interface, primarily aimed at enhancing interface stability to mitigate parasitic side reactions and electrolyte decompositions, particularly at elevated operating voltages and temperatures. Furthermore, its design should prioritize improving charge transfer kinetics at the cathode/electrolyte interface while ensuring optimal contact with cathode materials to minimize interfacial resistance. Moreover, the polymer-based surface coating must demonstrate both chemical and electrochemical stability. It should effectively shield cathode active particles from HF attacks and prevent phase transformations of cathode



materials during high-volume operation. Additionally, these coatings should accommodate volume expansions of cathode materials, thereby alleviating mechanical stresses and ultimately reducing particle cracking.

### 3. Advantages of polymer coatings on cathodes

Cathode materials are coated with metal oxides such as  $\text{Al}_2\text{O}_3$ ,  $\text{SiO}_2$ ,  $\text{ZrO}_2$ , and  $\text{TiO}_2$ .<sup>7,27-34</sup> However, it is well known that cathode materials undergo volume expansion and contraction during cycling. This results in mechanical stresses on these hard and brittle ceramic coatings, which may induce cracking and delamination of these coatings from the cathode surface. Therefore, the effectiveness of these coatings decreases with cycling due to the exposure of the fresh cathode surface to the electrolyte, leading to electrolyte decomposition and enhanced cell polarization. Moreover, ceramic coatings require post-annealing at elevated temperature ( $>600\text{ }^\circ\text{C}$ ), which may result in cation migration and cation mixing (interlayer diffusion), resulting in the deterioration of cell performance. Cathode materials can be processed with soft and sustainable polymer coatings at relatively lower temperatures. Hence, the chance of cation mixing in cathode particles during post-processing is minimized. Furthermore, as polymer-based coatings are flexible, the utilization of these coatings can prevent the delamination of the coatings from the cathode surface during extended cycling. Polymeric coatings, which generally achieve full surface coverage more readily, can prevent cracking by giving elastic support to the secondary particles. Moreover, polymer coatings are not prone to cracking (due to their elastic nature) by cyclic mechanical stresses. Such coatings can provide an excellent percolation network for electron and ion transfer for high-performance applications. For ASSBs, mixed ionic-electronic conducting polymeric materials form a good interfacial contact and ion-conducting network. Furthermore, polymers are known to be inert toward most acids, which can prevent HF chemical attack on cathode materials. The major benefits of polymer-based cathode coatings are listed as follows and demonstrated in Fig. 2.

- Morphology control (conformal, thin coating): during the coating of cathode materials with a ceramic-based coating, it is really challenging to control the quality of the coating (thickness and homogeneity). However, polymer coatings are comparatively easier to apply and form a homogeneous conformal coating on cathode active particles. Moreover, due to the ductile and flexible nature of these coatings, they can form ultra-conformal protective layers.

- Thermal stability: most of the polymers considered as cathode coatings have thermal stability in the range of 300–500 °C. This enables them to be good candidates for cathode surface coatings. Moreover, the thermal stability can further be tuned through the chemical modification of the polymers.

- Ionically conductive: in some cases, coating materials should be ionically conductive and electronically insulative to protect against the oxidation or reduction of electrolyte

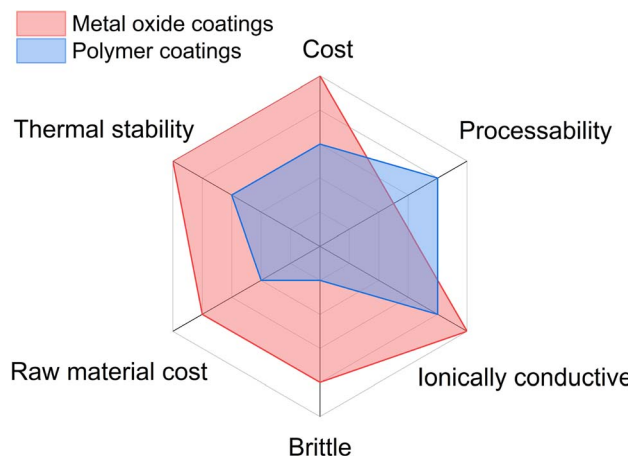


Fig. 2 The processability, properties and cost of ceramic and polymer-based cathode coatings are compared for lithium-ion batteries.

materials. Many polymers show excellent ionic conductivity when compared to metal oxide-based coating materials. Solid polymer electrolytes for solid-state batteries can also be employed as cathode coatings in lithium-metal batteries.

- Excellent electron percolation network: for ASSBs, the cathode composite should be mixed conducting. Due to the emergence of conductive polymers, they can provide an excellent ion and electron percolation network. Moreover, the electronic conductivities of these polymers can be increased by the incorporation of conductive particles such as carbon nanotubes (CNTs).

- Volume accommodation during (de)lithiation: due to the flexible/elastic nature of polymers, they can easily accommodate the volume changes in the cathodes during extensive cycling without delamination of the polymer coating. Hence, electrolyte decomposition can be minimized even at high voltage and temperature as the cathode surface remains protected in long-term cycling.

- Low processing costs: these coatings require low heat treatment temperatures and time, which can result in a considerable reduction in processing costs. In contrast, ceramic-based coatings which are currently being employed in commercial lithium-ion batteries require much higher time ( $>6\text{ h}$ ) and temperature ( $>600\text{ }^\circ\text{C}$ ). This can also reduce the possibility of metal-ion inter-diffusion at the cathode-coating phase boundary, which can result in the modification of the surface chemistry and thus might have a negative impact on the electrochemical performance of the coated cathodes.

- Trapping of metal ions: polymer coatings can reduce the cross-talk in lithium-ion batteries by trapping the transition metal ion, dissolved cathode electrolyte interphase (CEI) species, and the decomposed organic electrolyte constituents. The presence of a polymer coating on the cathode can mitigate or prevent these constituents from reaching the anode, thus reducing the cell aging related to anode–cathode crosstalk.

- Flexibility in coating design: the processing strategies are quite flexible. There have been different reports in the literature where the polymer coatings are achieved on cathode active



particles, cast electrodes (by infiltration of polymer solution) and a thin and uniform film coated on the metallic lithium anode.<sup>22,24,35</sup>

To summarize, we believe that polymer-based surface coatings have significant potential in shaping the future of Li-ion batteries and emerging ASSBs. Through chemical modifications, these coatings can achieve high ionic conductivities, thereby enhancing charge transfer at the cathode/electrolyte interface. Additionally, their flexible nature allows conformal surface coatings and accommodates volume expansions of cathode materials, effectively reducing mechanical stresses and mitigating particle cracking. Furthermore, these polymers can be modified to become inert to HF (hydrofluoric acid) and serve as HF scavengers, protecting the cathode active particles from its chemical attack. As a result, cathode particles with polymer coatings exhibit immense promise from a future perspective.

## 4. Possible challenges of polymers as cathode coatings

It should be kept in mind that polymer-based cathode coatings are not mature enough to replace ceramic-based metal oxide coatings for commercial applications. However, these polymer-based cathode coatings have significant potential for utilization in future battery systems. During the last few years, there has been a considerable increase in reports for polymer-based cathode coatings for lithium and sodium-ion batteries, which indicates the increasing interest of the battery community in polymer-based coatings. Moreover, these polymer coatings have shown considerable improvements in the electrochemical performance of cathodes.<sup>11,23,27,36-49</sup> However, there is a need for a more fundamental and mechanistic understanding before they can be successfully utilized in commercial applications.<sup>27</sup> As mentioned above, the recent interest in hybrid electrolytes (polymer/oxide or sulfide electrolytes) for all-solid-state batteries (ASSBs) has been increasing and the fundamental understanding of the polymer/ceramic interface is highly demandable. The ASSB community will benefit from the polymer-based coating for lithium anode and cathode particles for composite electrodes. However, there are several challenges that can hinder the pace of commercialization of polymer-based coatings in lithium-ion batteries. The possible challenges associated with polymer-based cathode coatings are listed below,

- Wide electrochemical stability window: for the successful utilization of polymers as cathode coatings, they should have a wide electrochemical stability window. These coatings should achieve good electrochemical stability *vs.* the cathode and electrolyte, especially at high operating voltages. Most of the polymer materials have a limited electrochemical stability window. However, the reported polymer coated cathode displayed better electrochemical performances compared to the uncoated cathode (as discussed later). This might be due to the *in situ* formation of a protective layer at the cathode/coating interface and thus can have the ability to protect these high

voltage cathodes against potential parasitic reactions with the electrolyte.

- Chemically stable with high voltage cathodes: the polymer coatings should be chemically stable with high voltage cathodes, especially when in contact with de-lithiated cathodes and at higher operating temperatures.

- Ionically and electronically conductive: to achieve improved electrochemical charge transfer kinetics, the coating surface should have good ionic and electronic conductivities. So, it can protect the cathode/electrolyte surface and at the same time, improve the ion and electron conductivity of composite electrodes for ASSBs. However, it is challenging to develop optimum coatings with excellent ionic and electronic conductivities simultaneously.

- Stable during extended cycling: it is well accepted that with extended cycling, the cathode surface and coating surface are prone to damage due to aging. However, the development of polymer coatings that could withstand extensive long-term cycling will be a challenge.

- Compatible with organic-based electrolytes: the polymer coatings should be compatible with organic-based liquid electrolytes. Since there is hardly any literature present which shows the stability of surface coatings themselves in organic-based liquid electrolytes, it is difficult to comment on the chemical stability of coatings during cycling. However, the coatings should be very stable and shouldn't show any unwanted side reactions with the liquid electrolytes. Otherwise, the purpose of surface coatings would be lost.

To summarize, while polymers present an appealing choice for cathode material coatings, they must overcome several challenges. Many polymers lack electrochemical stability at elevated voltages, necessitating the development or optimization of new polymers that are chemically and electrochemically stable, particularly at higher voltages. Additionally, polymer coatings should facilitate the conduction of both ions and electrons. Furthermore, they should demonstrate long-term stability during cycling, resisting delamination or decomposition to minimize interfacial kinetics. Finally, they should be compatible with both liquid and solid electrolytes.

## 5. Morphology of polymer-based cathode coatings

Due to the flexible nature of polymers, which can form thin conformal coatings on cathode materials, polymer coatings can improve cathode performance in terms of long-term cycling, rate capability, and safety.<sup>24-26,44,45,50-53</sup> The crystalline and amorphous coating layers were formed depending on the preparation techniques and types of polymer materials used.<sup>24-26,44,45,50-53</sup> Fig. 3 shows the morphologies of various polymer coatings on the cathode materials. Xu *et al.* developed ultra-conformal protective coatings using poly(3,4-ethylene dioxythiophene) (PEDOT) on Ni-rich LiNi<sub>0.85</sub>Co<sub>0.1</sub>Mn<sub>0.05</sub>O<sub>2</sub> (Ni-rich) and Li-rich Li<sub>1.2</sub>Mn<sub>0.54</sub>Ni<sub>0.13</sub>Co<sub>0.13</sub>O<sub>2</sub> (LMR-TMO).<sup>26</sup> The PEDOT improved lithium-ion and electron transport due to its mixed conductivity properties and reduced interfacial



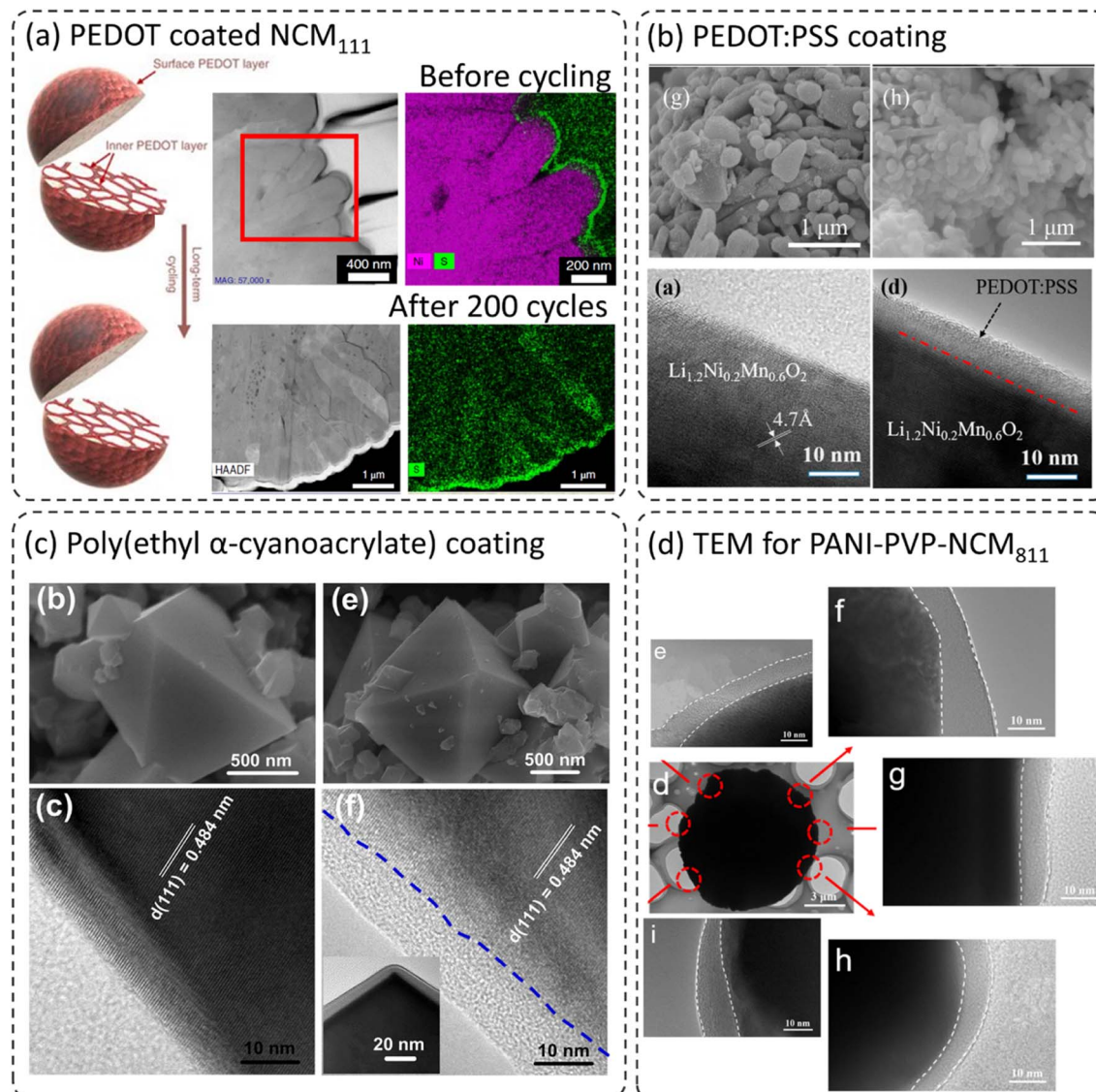


Fig. 3 (a) STEM-HAADF images of bare and PEDOT coated NCM<sub>111</sub>,<sup>26</sup> reproduced from ref. 26 with permission from Nature Portfolio, copyright 2019, (b) TEM images for different regions of a particle for PANI–PVP coated NCM<sub>811</sub>,<sup>46</sup> reproduced from ref. 46 with permission from American Chemical Society, copyright 2016, (c) SEM and TEM images for conformal poly(ethyl  $\alpha$ -cyanoacrylate) (PECA) coating on LiNi<sub>0.5</sub>Mn<sub>1.5</sub>O<sub>4</sub>,<sup>49</sup> reproduced from ref. 49 with permission from Elsevier, copyright 2017, (d) TEM images for PANI coated NCM<sub>811</sub>,<sup>23</sup> reproduced from ref. 23 with permission from American Chemical Society, copyright 2019.

resistance. Here, the oxidative chemical vapor deposition (oCVD) technique was adapted to form a protective coating layer both on the secondary and primary particles as shown schematically in Fig. 3a. The scanning transmission electron microscopy high-angle annular dark-field (STEM-HAADF) images along with elemental mapping show a very thin crystalline and conformal coating developed on the primary and secondary particles. Such a coating is generally difficult to achieve with ceramic-based coatings. The postmortem analysis indicated that even with long-term cycling, the PEDOT coating is still present without any visible changes in its morphology and the cathode material did not show any crack formation. It can be concluded that the presence of the PEDOT film significantly suppressed the layered to spinel/rock-salt phase transformation and retarded the mechanical cracking between

different primary particles. It is shown that the cycling and thermal stability of Ni-rich and LMR-TMO cathodes were considerably improved due to the stabilization of the cathode–electrolyte interphase. Wu *et al.* coated a lithium-rich Li<sub>1.2</sub>–Ni<sub>0.2</sub>Mn<sub>0.6</sub>O<sub>2</sub> cathode with the composite poly(3,4-ethylenedioxythiophene):poly(styrenesulfonate) (PEDOT:PSS) using the wet coating method as shown in the scanning electron microscopy (SEM) and TEM images in Fig. 3b.<sup>46</sup> This technique formed an amorphous coating layer in the range of 5–20 nm depending on the amounts of coating precursors used. The PEDOT:PSS composite exhibits high conductivity ( $\sim 10\text{--}10^2 \text{ S cm}^{-1}$ ) and excellent thermal and electrochemical stability.<sup>47,48</sup> The SEM images display no visible change on the secondary particle surface. Note that it is quite challenging to see a coated layer using SEM. However, the instigation of



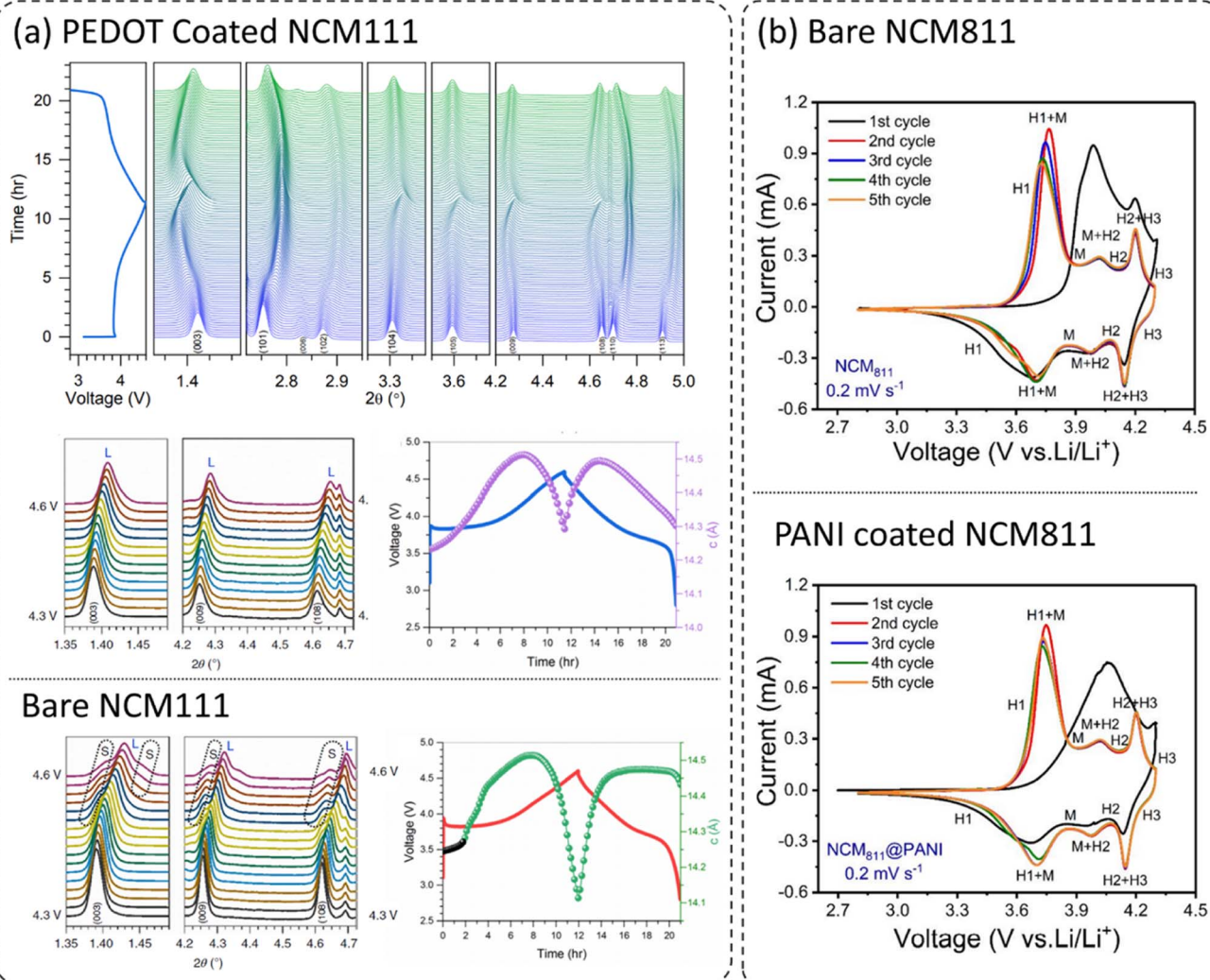


Fig. 4 (a) *In situ* HEXRD patterns of the PEDOT coated NCM<sub>111</sub> cathode during the 1st charge/discharge cycle within 2.8–4.6 V. Later, the HEXRD patterns of bare and PEDOT coated NCM<sub>111</sub> in the voltage region of 4.3–4.6 V during the charge at C/10, and the change in the lattice parameter 'c' as a function of charge/discharge time. L and S correspond to the layered and spinel phases, respectively,<sup>26</sup> reproduced from ref. 26 with permission from Nature Portfolio, copyright 2019, (b) CV curves for the five cycles at 0.2 mV s<sup>-1</sup> (2.8–4.3 V) for bare and PANI coated NCM<sub>811</sub>,<sup>23</sup> reproduced from ref. 23 with permission from American Chemical Society, copyright 2019.

focused ion beam milling (FIB) or elemental mapping can give a better idea about the coating layer. Nevertheless, TEM images clearly distinguish the difference between bare and PEDOT:PSS coated Li<sub>1.2</sub>Ni<sub>0.2</sub>Mn<sub>0.6</sub>O<sub>2</sub> surfaces. A thin, amorphous, and conformal coating layer can be seen with a thickness of around 8 nm. Here, the 3 wt% PEDOT:PSS coated cathode showed the best electrochemical performance in terms of cycling and rate capability. The improved performance was directly linked to the high conductivity of the PEDOT:PSS coated layer and to the formation of a stable cathode-electrolyte interphase (CEI) during long-term cycling. Liu *et al.* synthesized a poly(ethyl  $\alpha$ -cyanoacrylate) (PECA) coated high voltage spinel cathode LiNi<sub>0.5</sub>Mn<sub>1.5</sub>O<sub>4</sub> using an *in situ* polymerization reaction as shown in Fig. 3c.<sup>49</sup> The authors claim that the PECA behaves as a high voltage polymer electrolyte on the LNMO surface due to its high ionic conductivity. They emphasized the prevention of metal-ion dissolution from the cathode due to the PECA

coating. However, the SEM images show (Fig. 3c) no visible difference in surface morphology between the bare and PECA coated LNMO. This might be due to the limitations of SEM imaging. However, the TEM images show a thin and homogeneous PECA layer on the cathode sample. The coating thickness is around 10 nm and is amorphous in nature. The authors were able to show by TEM analysis that the coating treatment has no visible effect on the intrinsic lattice structure of the coated LNMO. Gan *et al.* developed a thin polyaniline (PANI) and polyaniline-polyvinylpyrrolidone (PANI-PVP) composite coating on high NiLiNi<sub>0.8</sub>Co<sub>0.1</sub>Mn<sub>0.1</sub>O<sub>2</sub> (NCM<sub>811</sub>) (Fig. 3d).<sup>23</sup> Here, the PVP layer was introduced as an inductive agent to improve the adhesion of PANI and the NCM<sub>811</sub> cathode and thus, to develop a homogeneous thin coating. As seen in the TEM images, NCM<sub>811</sub>@PANI-PVP shows homogeneous coverage with the coating layer with a coating thickness of around 10 nm. The TEM images from different parts of a particle show complete

coverage of PANI–PVP without any uncoated or uneven regions. NCM<sub>811</sub>–PANI–PVP showed excellent cycling and rate capability when compared with bare NCM<sub>811</sub>.

## 6. Structural stability with polymer-based cathode coatings

It is well known that layered oxide cathodes LiNi<sub>1-x-y</sub>Co<sub>x</sub>Mn<sub>y</sub>O<sub>2</sub> (NCM) may undergo structural transformations with loss of oxygen from the lattice while cycled under different operating conditions. The most favorable transformation is from layered oxide to spinel and/or rock-salt phases originating at the surfaces of the cathodes.<sup>11,27,36,37,39–41,54,55</sup> However, it is reported that the incorporation of dopants into the crystal lattice or surface coatings of cathodes can mitigate the structural transformations.<sup>8,36,56–64</sup> Therefore, doping and surface coatings are considered effective and viable approaches to improving the performance of layered oxide LiNi<sub>1-x-y</sub>Co<sub>x</sub>Mn<sub>y</sub>O<sub>2</sub> (NCM) cathodes. Xu *et al.* covered the layered oxide LiNi<sub>1/3</sub>Co<sub>1/3</sub>Mn<sub>1/3</sub>O<sub>2</sub> (NCM<sub>111</sub>) with a thin homogeneous PEDOT coating utilizing the oxidative chemical vapor deposition (CVD) process and the reported coating process suppressed the phase transformation. Similarly, another report has achieved the coating on the primary particles and demonstrated improved electrochemical performance, mitigation of structural transformation, enhancement in thermal safety, and mitigation of crack formation in the cathode during extensive cycling.<sup>36</sup> Fig. 4a shows the *in situ* high-energy X-ray diffraction (HEXRD) patterns of the PEDOT coated NCM<sub>111</sub> cathode during the 1st charge/discharge cycle within 2.8–4.6 V, clearly displaying high structural reversibility.<sup>26</sup> The comparison of *in situ* HEXRD patterns of PEDOT–NCM<sub>811</sub> and bare NCM<sub>811</sub> (not shown here) reveals clear differences in structural evolutions during the first charge/discharge cycle. The XRD peaks for bare NCM<sub>811</sub> couldn't return to the same positions, indicated by the (003), (101), (102), (108), (110), and (113) peaks, after the first charge/discharge cycle, clearly indicating some irreversible structural changes in the cathode. Moreover, high-Ni layered oxides LiNi<sub>1-x-y</sub>Co<sub>x</sub>Mn<sub>y</sub>O<sub>2</sub> (NCM) (Ni > 60%) are structurally less stable and thus, undergo severe structural changes during cycling.<sup>65–69</sup> These structural changes and transformations are more pronounced at higher operating voltages and temperatures.<sup>70–73</sup> This can be seen by the emergence of weak shoulder peaks (indicated as S) at high voltage (>4.3 V) during the first charge for bare NCM<sub>111</sub>. These weak shoulder peaks correspond to the formation of the spinel phase (abbreviated as S) with the *Fd*<sup>3</sup>*m* space group, which is associated with the loss of oxygen from the crystal lattice. In comparison, PEDOT coated NMC<sub>111</sub> didn't show the formation of any secondary phase. Mechanical stresses are created in the primary and secondary particles, thus leading to mechanical cracking of the bare cathode material, and suppressed in the coated cathode. The positive effect of polymer coatings on structural and cycling stability can also be analyzed by comparing the cyclic voltammograms (CV) of bare and coated cathodes. Fig. 4b compares the CV for the first five cycles at 0.2 mV s<sup>-1</sup> (2.8–4.3 V) for bare and PANI coated NCM<sub>811</sub>.<sup>23</sup> These

layered oxide materials display a series of phase transformations such as hexagonal to monoclinic (H1  $\leftrightarrow$  M), monoclinic to hexagonal (M  $\leftrightarrow$  H2), and hexagonal to hexagonal (H2  $\leftrightarrow$  H3). There is a drop in the oxidation peak corresponding to (H1  $\leftrightarrow$  M) during successive cycles for both bare and PANI-coated NCM<sub>811</sub>. However, the shape and peak intensity for PANI-coated NCM<sub>811</sub> in comparison to bare NCM<sub>811</sub> show better electrochemical reversibility and structural stability. This would be more pronounced at higher cutoff voltages and higher operating temperatures, thus demonstrating the beneficial role of PANI coating in NCM<sub>811</sub> cathodes.

## 7. Types of polymer-based cathode coatings

Every polymer material has its inherent physical, chemical, mechanical, ionic, and electronic transport properties and electrochemical stability. Their coating properties appear to be different from one type of polymer material to another. The important classes of polymer-coated cathodes are discussed and analyzed in detail individually.<sup>26,51,74–90</sup>

### 7.1 Poly(3,4-ethylenedioxythiophene) (PEDOT)

PEDOT is considered a potential cathode coating material due to its high ionic and electronic transport properties.<sup>26,83,91</sup> It will be an ideal coating material in composite cathodes for ASSBs due to the favorable transport and mechanical properties. Xu *et al.* reported an ultra-conformal thin PEDOT coating on different types of layered oxide cathode materials including LiNi<sub>1/3</sub>Co<sub>1/3</sub>Mn<sub>1/3</sub>O<sub>2</sub> (NCM<sub>111</sub>), Ni-rich LiNi<sub>0.85</sub>Co<sub>0.1</sub>Mn<sub>0.05</sub>O<sub>2</sub>, and Li-rich Li<sub>1.2</sub>Mn<sub>0.54</sub>–Ni<sub>0.13</sub>Co<sub>0.13</sub>O<sub>2</sub>.<sup>26</sup> The thickness of the PEDOT coating was controlled by the OCVD reaction time X-PEDOT@NCM<sub>111</sub> (where X refers to the OCVD deposition time in minutes). Fig. 5a-i show the morphology of PEDOT–NMC<sub>111</sub> cathode materials at various reaction times. The coating thickness increased from 7 nm to 18 nm for 20 minutes and 80 minutes, respectively. Nonetheless, it is important to note that all the coated cathodes show conformal coating morphology without any irregularities. Such coatings are highly desirable for the good passivation of the cathode from the electrolyte and faster kinetics. The cathodes were cycled between 3.0 and 4.6 V at 1C for 200 cycles as shown in Fig. 5a-ii. Due to the higher upper cutoff voltage of 4.6 V, bare NCM<sub>111</sub> displays fast capacity fading and retains only 47.7% of its initial discharge capacity after 200 cycles. However, it is worth noting that all the coated NCM<sub>111</sub> materials displayed substantial improvement in capacity retention. 60-PEDOT–NCM<sub>111</sub> with a coating thickness of around 20 nm displayed the best capacity retention of around 91.1%. It is well known that the layered oxide LiNi<sub>1-x-y</sub>Co<sub>x</sub>Mn<sub>y</sub>O<sub>2</sub> (NCM) and spinel oxides LiMn<sub>2</sub>O<sub>4</sub> (LMO) and LiNi<sub>0.5</sub>Mn<sub>1.5</sub>O<sub>4</sub> (LNMO) materials undergo an HF generation–corrosion loop, which directly exposes them to the electrolyte during long-term cycling, resulting in continuous transition metal cation dissolution.<sup>27,55,57,63,92–97</sup> To confirm the HF-scavenging behavior of the PEDOT coating, the PEDOT–NCM<sub>111</sub> cathodes were mixed with a HF bearing electrolyte and the corresponding HF concentration was monitored after 48 h (not shown here). The overall HF



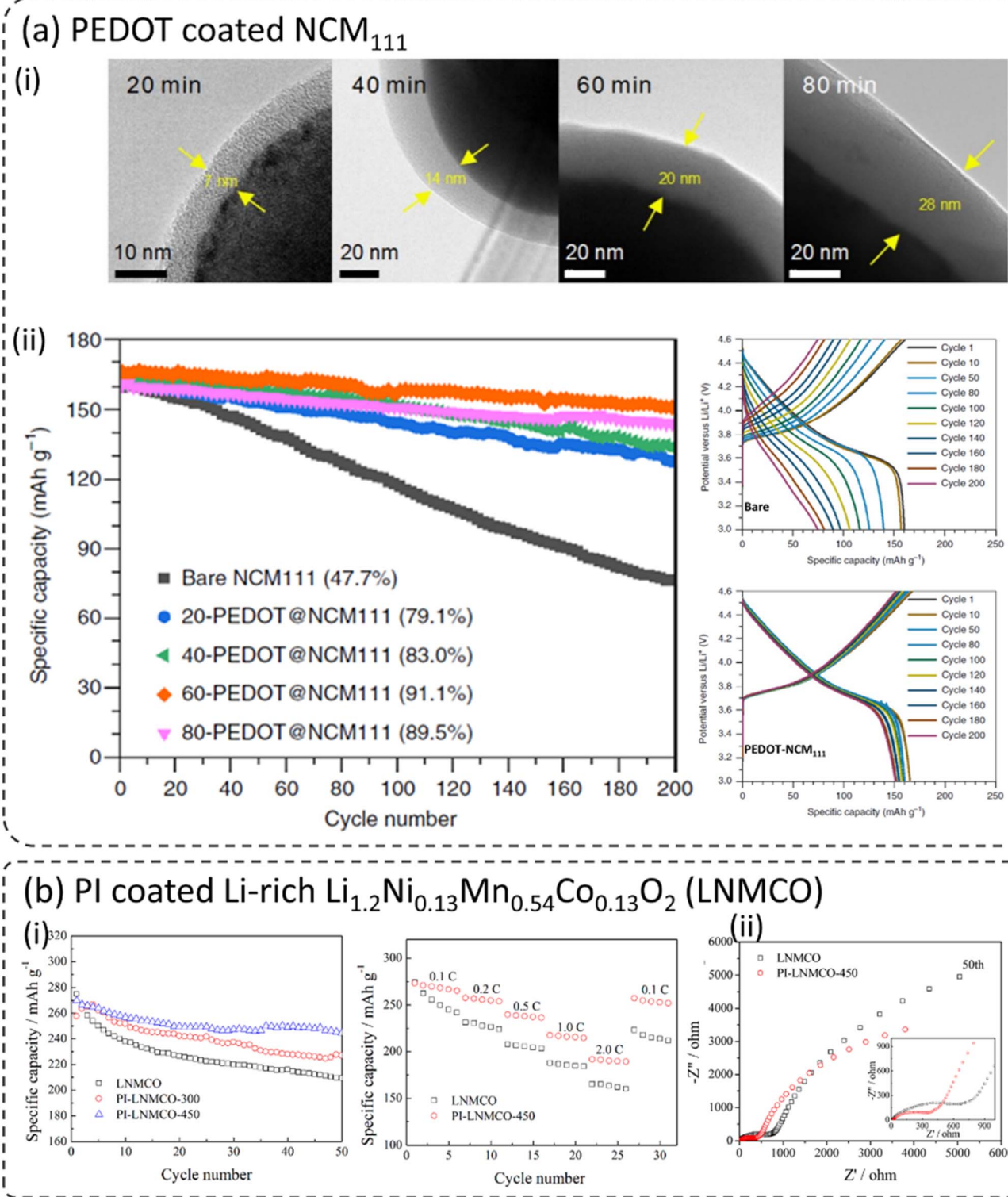


Fig. 5 (a) PEDOT coated NCM<sub>111</sub> using oxidative chemical vapour deposition (oCVD), (i) TEM images of PEDOT coated NCM<sub>111</sub> at different oCVD coating times, (ii) capacity retention of bare and PEDOT coated NCM<sub>111</sub>Li half-cells at 1C and corresponding charge/discharge curves, (iii) the effect of PEDOT coating on HF scavenging and transition metal (Ni, Co, and Mn) dissolution after 200 cycles,<sup>26</sup> reproduced from ref. 26 with permission from Nature Portfolio, copyright 2019, (b) polyimide (PI) coated Li-rich Li<sub>1.2</sub>Ni<sub>0.13</sub>Mn<sub>0.54</sub>Co<sub>0.13</sub>O<sub>2</sub> (LNMCO), (i) cycling and rate capability of bare and PI coated LNMCO, (iii) EIS spectra before and after the 50th cycle for based and PI coated LNMCO,<sup>78</sup> reproduced from ref. 78 with permission from American Chemical Society, copyright 2014.

concentration was reduced by around 50% due to the 60-PEDOT-NCM<sub>111</sub> coating. Furthermore, the transition metal dissolution (Ni, Co, and Mn) was found to be considerably low with the application of the PEDOT coating.

## 7.2 Polyimide (PI)

Polyimide (PI) was used to coat various cathode materials and their electrochemical performances were discussed therein.<sup>77,78,98,99</sup> Jie *et al.* coated Li-rich Li<sub>1.2</sub>Ni<sub>0.13</sub>Mn<sub>0.54</sub>Co<sub>0.13</sub>O<sub>2</sub> (LNMCO) with polyimide (PI) (Fig. 5b) and heat-treated at two different temperatures 300 and 450 °C, respectively.<sup>78</sup> Both coated materials showed a thin and homogeneous coating on the LNMCO surface and exhibited much-improved cycling

stability compared to bare LNMCO as shown in Fig. 5b-i. The sample coated at 450 °C exhibited better capacity retention (90.6%) compared to the bare sample (78%) after 50 cycles. The PI-coated LNMCO displayed enhanced rate capability due to the improved charge transfer kinetics at the cathode–electrolyte interface. Interestingly, the initial cell resistance of the coated sample is higher than that of the bare sample. However, after several cycles, the opposite trend was observed (Fig. 5b-ii). This might be due to the slow wetting and impregnation of the electrolyte into the polymer coating layer, thus enabling proper contact between the cathode and electrolyte. Therefore, it clearly shows that the presence of PI on the surface of LNMCO

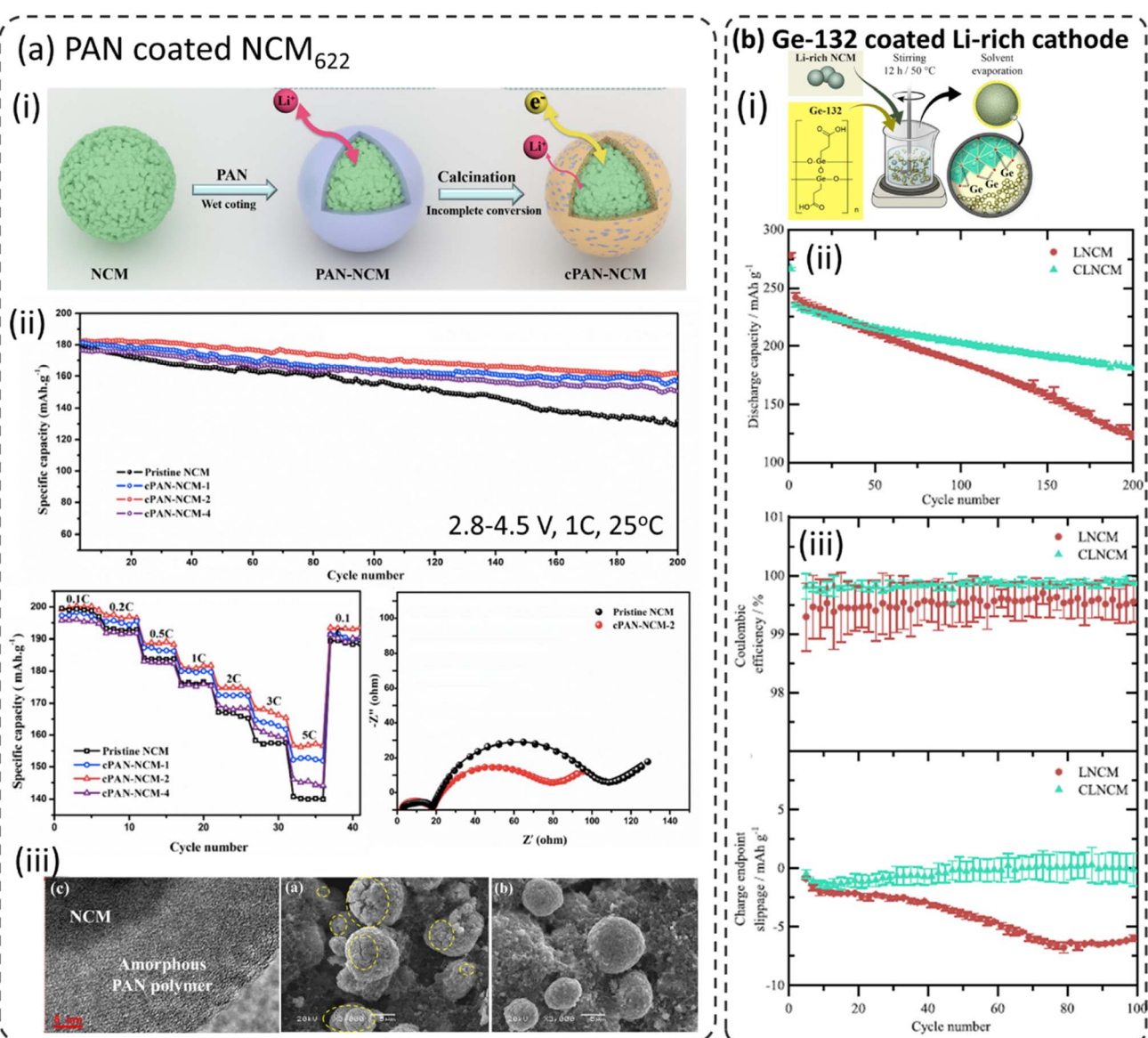


Fig. 6 (a) PAN coated NCM<sub>622</sub>, (i) schematic illustration of the cPAN coated NCM<sub>622</sub> cathode, (ii) electrochemical performance including cycling at 1C between 2.8 and 4.5 V at 25 °C, rate capability and electrochemical impedance spectra after the 30th cycle in the charged state (4.5 V), (iii) SEM images of bare and PAN-NCM<sub>622</sub> long-term cycling (100 cycles),<sup>86</sup> reproduced from ref. 86 with permission from Elsevier, copyright 2019. (b) carboxyethylgermanium (Ge-132) coating on the Li-rich NCM cathode, (i) schematic representation for the process employed for coating, (ii) long-term cycling performance, (iii) coulombic efficiencies and cumulative charge endpoint slippage vs. cycle number for bare and Ge-132 coated Li-rich NCM in NCM|graphite full-cells,<sup>100</sup> reproduced from ref. 100 with permission from The Electrochemical Society, copyright 2020.



effectively stabilizes the cathode–electrolyte interface, leading to better electrochemical performance.

### 7.3 Polyacrylonitrile (PAN)

It is reported that polyacrylonitrile (PAN) was converted to a cyclized polyacrylonitrile (cPAN) layer while heat-treated and calcinated (Fig. 6a-i) and expected to have better electronic conductivity.<sup>14–16</sup> Noting that the flexible and elastic polymeric coatings not only suppress the side reactions at the cathode–electrolyte interface but also suppress the volume expansions of the cathodes during (de)lithiation and crack formation on the cathode particle during long-term cycling. The resulting cPAN coated NCM<sub>622</sub> exhibited enhanced electrochemical performance as shown in Fig. 6a-ii. The cPAN thickness plays an important role in high-rate performances. Various amounts of PAN were employed to coat NCM<sub>622</sub> and it turns out that the 2% PAN coated sample exhibits better performances than either higher or lower coating thickness. Electrochemical impedance spectroscopy (EIS) analysis (after 30 charge/discharge cycles) confirms that cPAN–NCM samples have much smaller charge transfer resistance ( $R_{ct}$ ) than bare NCM. The increased  $R_{ct}$  for bare NCM is due to the formation of an unstable cathode–electrolyte interphase (CEI) by the decomposition of electrolytes at higher operating voltage. Furthermore, the presence of cPAN mitigated the crack formation in cathode particles during long-term cycling (100 cycles) as shown in SEM images in Fig. 6a-iii.

### 7.4 Carboxyethylgermanium (Ge-132)

Becker *et al.* reported the utilization of carboxyethyl germanium (Ge-132) to coat a Li-rich Li<sub>1.15</sub>Ni<sub>0.15</sub>Co<sub>0.15</sub>Mn<sub>0.55</sub>O<sub>2</sub> (Li-rich NCM) cathode material using the sol–gel process as shown schematically in Fig. 6b-i.<sup>100</sup> As mentioned above the Li-rich layered oxide cathode (Li<sub>2</sub>MnO<sub>3</sub>–LiMO<sub>2</sub>) suffers from poor cycling stability, rapid voltage fading, and structural degradation during extensive cycling and its electrochemical performances were improved through Ge-132 coating.<sup>101–108</sup> Noting that the Ge-132 coated Li-rich NCM showed much-improved capacity retention (92%) when compared to bare Li-rich NCM (88%) after 200 cycles (Fig. 6b-ii). The coulombic efficiency (CE) and accumulated charge endpoint slippage *vs.* the cycle number during the first 100 cycles are displayed in Fig. 6b-iii. These parameters give more insights into the impact of parasitic reactions. Ge-132 coated Li-rich NCM shows much fewer parasitic reactions as indicated by higher and stable coulombic efficiency values compared to bare Li-rich NCM. Moreover, the cells with Ge-132-coated Li-rich NCM show a higher (less negative) charge endpoint slippage compared to uncoated Li-rich NCM. These results indicate the stabilization of the cathode material surface with Ge-132 coating.

### 7.5 Polyaniline (PANI) and polyvinylpyrrolidone–polyaniline (PVP–PANI) composite coating

A PVP–PANI-based composite homogeneous thin (3–6 nm) coating layer was formed on the Ni-rich layered oxide LiNi<sub>0.8</sub>Co<sub>0.1</sub>Mn<sub>0.1</sub>O<sub>2</sub> (NCM<sub>811</sub>) as shown in Fig. 7a-i.<sup>35,86,87</sup> The presence of the PVP intermediate layer improved the bonding and morphology of the PANI layer on NCM<sub>811</sub> and protected the

unstable NCM<sub>811</sub> in the charged state against electrolyte corrosion. In addition, the PANI layer improved the charge transfer kinetics, especially at higher C-rates, due to its excellent ion transport properties. Rate performances are also considerably enhanced as shown in Fig. 7a-ii. It should be noted that bare NCM<sub>811</sub> shows a rapid increase in charge transfer resistance ( $R_{ct}$ ) after 100 cycles compared to PANI–NCM<sub>811</sub> and PANI–PVP–NCM<sub>811</sub> samples as shown in Fig. 7a-iii. The Ni-rich layered oxides LiNi<sub>1-x-y</sub>Co<sub>x</sub>Mn<sub>y</sub>O<sub>2</sub> (NCM, Ni > 60%) have serious safety concerns, especially in a charged state.<sup>42,80–87</sup> PANI–PVP–NCM<sub>811</sub> shows improvement in safety characteristics with the increase of onset decomposition temperature in the presence of the coating.

### 7.6 Lithium polyacrylate (LiPAA)–silane-coupling agent (KH550) composite coating

The polyacrylate (PAA) and silane-coupling agent (KH550) have been used to form a composite coating on Ni-rich LiNi<sub>0.8</sub>–Co<sub>0.15</sub>Al<sub>0.05</sub>O<sub>2</sub> (NCA) as shown schematically in Fig. 7b-i.<sup>24,85</sup> The advantages and disadvantages of PAA are that it converts into lithium polyacrylate (LiPAA) and provides excellent Li<sup>+</sup> conductivity and high voltage stability. Furthermore, it can suppress electrolyte corrosion by forming an outer cross-linked layer. However, it might reduce the capacity of the full cells due to the consumption of Li by PAA. As seen in Fig. 7b-ii, the cycling performance of coated NCA improves long-term cycling at 1C and displayed the best capacity retention. After the 100th cycle, the charge transfer resistance ( $R_{ct}$ ) of bare NCA increased significantly compared to the coated sample. Furthermore, bare NCA shows particle cracking after long-term cycling (Fig. 7b-iii) and shows large variations in lattice spacings, which revealed the layered to rock-salt phase transformation. This resulted in large volume changes and thus the intergranular cracking and pulverization of NCA. On the other hand, coated NCA displayed a very thin and homogeneous layer (~3–5 nm) of the rock-salt phase on the particle surface. This clearly supports the conclusion that the presence of the surface coating mitigated the phase transformation.

To conclude, the literature suggests that polymer-based surface coatings applied to cathode materials should be both uniform and conformable. Thin coatings tend to enhance the electrochemical performance of coated cathodes, while thicker coatings may detrimentally impact the performance by increasing interfacial resistance. However, opting for a suitable polymer coating poses a formidable challenge.

## 8. Comparison of electrochemical properties with and without polymer coatings

The electrochemical performances of electrode materials with and without polymer coatings are compared in Table 1. It can be seen from Table 1 that the cycling stability can be greatly improved with polymer coatings in all cathode materials, even though most of the polymer materials are electrochemically unstable at higher voltages. The better electrochemical



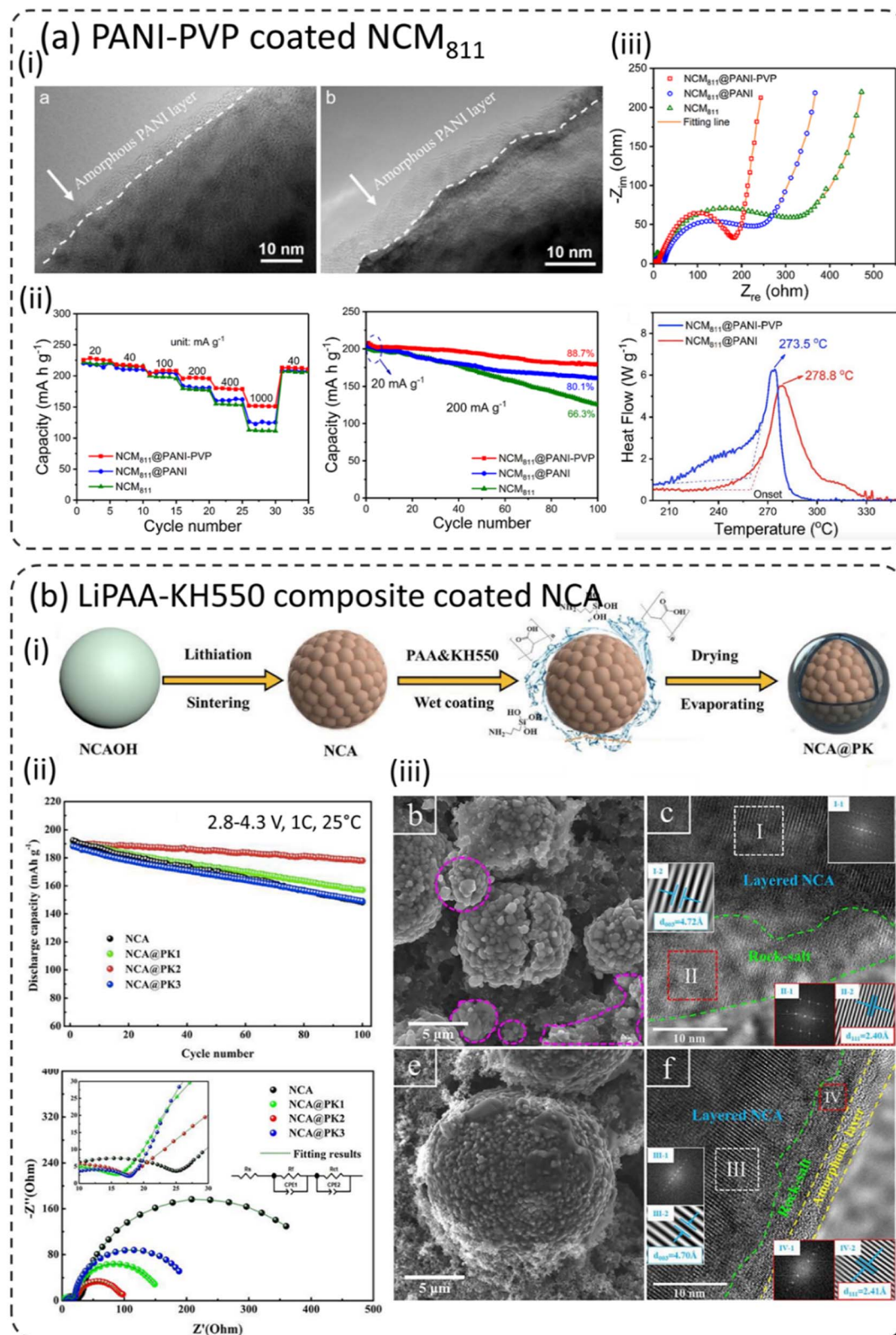


Fig. 7 (a) PANI-PVP coated NCM<sub>811</sub>, (i) TEM image of the PANI-PVP coated NCM<sub>811</sub> cathode material, (ii) rate capability and cycling performance comparison, and (iii) electrochemical impedance spectra (EIS) after the 100th cycle and DSC profiles of bare NCM<sub>811</sub> and PANI-PVP-NCM<sub>811</sub>,<sup>35</sup> reproduced from ref. 35 with permission from American Chemical Society, copyright 2019, (b) lithium polyacrylate (LiPAA) coated Ni-rich LiNi<sub>0.8</sub>Co<sub>0.15</sub>Al<sub>0.05</sub>O<sub>2</sub> (NCA), (i) schematic illustration of the PAA coated NCA cathode, (ii) cycling and EIS spectra of bare and PAA-NCA cathodes after 100 cycles, and (iii) SEM and TEM images of bare and NCA@PK2 cathode particles after 100 cycles,<sup>85</sup> reproduced from ref. 85 with permission from Wiley, copyright 2020.



Table 1 The comparison of the electrochemical performances of different polymer-coated cathode materials in Li-ion batteries

Coating material	Cathode material (coating wt%)	Electrochemical performance			Ref.
		Initial capacity → final capacity (mA h g <sup>-1</sup> )	capacity retention (%)	C-rate, total cycles	
Polypprole (PPy)	LiNi <sub>0.2</sub> Co <sub>0.2</sub> Mn <sub>0.3</sub> O <sub>2</sub> (NCM523) (5 wt% PPy)	184 → 76, 41.10%@1C, 200 cycles	190 → 128, 67.20%@1C, 200 cycles	81	
	LiNi <sub>0.8</sub> Co <sub>0.1</sub> Mn <sub>0.1</sub> O <sub>2</sub> (NCM811) (5 wt% PPy)	178 → 117, 65.8%@1C, 200 cycles	181 → 137, 76.1%@1C, 200 cycles	109	
	LiNi <sub>0.5</sub> Mn <sub>1.5</sub> O <sub>4</sub> (LNMO) (5 wt% PPy)	116 → 94, 76.7%@1C, 300 cycles	118 → 112.9, 91.0%@1C, 300 cycles	82	
	LiNi <sub>0.8</sub> Co <sub>0.15</sub> Al <sub>0.05</sub> O <sub>2</sub> (NCA) (2 wt% PPy)	173 → 124, 71.6%@1C, 100 cycles	196 → 174, 88.9%@1C, 100 cycles	80	
Polyimide (PI)	Li <sub>1.2</sub> Ni <sub>0.13</sub> Mn <sub>0.54</sub> Co <sub>0.13</sub> O <sub>2</sub>	277 → 210, 78.0%@0.1C, 50 cycles	270 → 244, 90.6%@0.1C, 50 cycles	78	
	LiCoO <sub>2</sub> (LCO)	200 → 88, 44.0%@0.5C, 50 cycles (3.0–4.6 V)	200 → 128, 64.0%@0.5C, 50 cycles (3.0–4.6 V)	98	
	LiNi <sub>0.5</sub> Mn <sub>1.5</sub> O <sub>4</sub> (LNMO)	124 → 98, 79.0%@1C, 50 cycles (55 °C)	126 → 120, 95.5%@1C, 50 cycles (55 °C)	99	
	LiNi <sub>1/3</sub> Co <sub>1/3</sub> Mn <sub>1/3</sub> O <sub>2</sub> (NCM111) (10 nm PI)	180 → 95, 52.0%@1C, 50 cycles (2.8–4.8 V)	180 → 120, 66.0%@1C, 50 cycles (2.8–4.8 V)	75	
Polyaniline (PANI)	Li <sub>3</sub> N <sub>2</sub> (PO <sub>4</sub> ) <sub>3</sub>	109 → 101, 92.1%@0.1C, 30 cycles	130.7 → 128.5, 98.3%@0.1C, 30 cycles	89	
	LiNi <sub>0.8</sub> Co <sub>0.1</sub> Mn <sub>0.1</sub> O <sub>2</sub> (NCM811) (3 wt% PANI)	195 → 175, 90.0%@1C, 80 cycles	193 → 186, 96.2%@1C, 80 cycles	74	
	LiNi <sub>0.5</sub> Mn <sub>1.5</sub> O <sub>4</sub> (LNMO)	107 → 18, 16.4%@1C, 100 cycles (55 °C)	113 → 107, 94.5%@1C, 100 cycles (55 °C)	51	
	LiNi <sub>0.8</sub> Co <sub>0.1</sub> Mn <sub>0.1</sub> O <sub>2</sub> (NCM811)	190 → 126, 66.3%@200 mA g <sup>-1</sup> , 100 cycles	199 → 160, 80.4%@200 mA g <sup>-1</sup> , 100 cycles	23	
	LiNi <sub>0.8</sub> Co <sub>0.1</sub> Mn <sub>0.1</sub> O <sub>2</sub> (NCM811)	196 → 103, 53.6%@1C, 100 cycles (55 °C)	202 → 157, 77.1%@1C, 100 cycles (55 °C)	90	
	LiNi <sub>0.5</sub> Mn <sub>1.5</sub> O <sub>4</sub> (LNMO) (3 wt% PEDOT)	127 → 107, 83.4%@1C, 200 cycles	129 → 121, 92.8%@1C, 200 cycles	74	
	LiNi <sub>1/3</sub> Co <sub>1/3</sub> Mn <sub>1/3</sub> O <sub>2</sub> (NCM111)	160 → 76, 47.4%@1C, 200 cycles	166 → 151, 91.1%@1C, 200 cycles	26	
	LiNi <sub>0.85</sub> Co <sub>0.1</sub> Mn <sub>0.05</sub> O <sub>2</sub>	151 → 81, 54.0%@1C, 100 cycles	178 → 161, 91.0%@1C, 100 cycles	26	
	Li <sub>1.2</sub> Mn <sub>0.54</sub> Ni <sub>0.13</sub> Co <sub>0.13</sub> O <sub>2</sub>	240 → 128, 53.0%@0.1C, 50 cycles	240 → 221, 93.0%@0.1C, 50 cycles	26	
	LiMn <sub>2</sub> O <sub>4</sub>	108 → 80, 74.1%@1C, 120 cycles	115 → 91, 79.1%@1C, 120 cycles	84	
	LiNi <sub>0.5</sub> Mn <sub>1.5</sub> O <sub>4</sub> (LNMO) (3 wt% PEDOT)	122 → 81, 56.5%@0.2C, 200 cycles	125 → 115, 91.6%@0.2C, 200 cycles	91	
	Li <sub>3</sub> N <sub>2</sub> (PO <sub>4</sub> ) <sub>3</sub>	116 → 105, 90.3%@0.1C, 40 cycles	128 → 126, 98.1%@0.1C, 40 cycles	110	
	LiNi <sub>0.6</sub> Co <sub>0.2</sub> Mn <sub>0.2</sub> O <sub>2</sub> (NCM622) (2 wt% PAN)	180 → 132, 73.3%@1C, 200 cycles	182 → 162, 88.6%@1C, 200 cycles	86	
	LiNi <sub>0.5</sub> Mn <sub>1.5</sub> O <sub>4</sub> (LNMO) (2 wt% PAN)	120 → 94, 78.2%@1C, 200 cycles	122 → 111, 90.0%@1C, 200 cycles	87	
	LiCoO <sub>2</sub> (LCO)	185 → 162, 87.3%@0.7C, 300 cycles	182 → 172, 94.2%@0.7C, 300 cycles	88	
	LiNi <sub>0.5</sub> Mn <sub>1.5</sub> O <sub>4</sub> (LNMO)	125 → 94, 74.7%@1C, 100 cycles	122 → 112, 92.0%@1C, 100 cycles	49	
	LiNi <sub>0.6</sub> Co <sub>0.1</sub> Mn <sub>0.3</sub> O <sub>2</sub> (NCM613) (0.01 wt% PVP) (5 wt% PDMS) (2 week air storage)	158 → 112, 70.9%@0.5C, 250 cycles	155 → 126, 80.6%@0.5C, 250 cycles	111	
	LiNi <sub>0.8</sub> Co <sub>0.1</sub> Mn <sub>0.1</sub> O <sub>2</sub> (NCM811)	198 → 121, 61.9%@1C, 200 cycles	177 → 128, 72.9%@1C, 200 cycles	112	
		188 → 96, 51.2%@1C, 100 cycles	175 → 155, 88.8%@1C, 100 cycles	113	
Polyacrylonitrile (PAN)					
Poly(ethyl $\alpha$ -cyanoacrylate)	Li <sub>1.15</sub> Ni <sub>0.15</sub> Co <sub>0.15</sub> Mn <sub>0.35</sub> O <sub>2</sub> (5 wt% Ge-132)	240 → 122, 50.8%@0.5C, 200 cycles	234 → 180, 76.9%@0.5C, 200 cycles	100	
Poly(4-vinylphenol) (PVP)					
Polydimethyl-siloxane (PDMS)	LiNi <sub>0.8</sub> Co <sub>0.1</sub> Mn <sub>0.1</sub> O <sub>2</sub> (NCM811)	180 → 44, 24.4%@0.2C, 80 cycles	220 → 140, 63.6%@0.2C, 80 cycles	114	
Pyrazine-linked covalent organic framework (Pyr-2D)	Li[Ni <sub>0.5</sub> Co <sub>0.3</sub> Mn <sub>0.2</sub> O <sub>2</sub> (NCM532) (0.5 wt% LIVING)]	159 → 105, 66.2%@0.2C, 100 cycles	156 → 127, 80.7%@0.2C, 100 cycles	115	

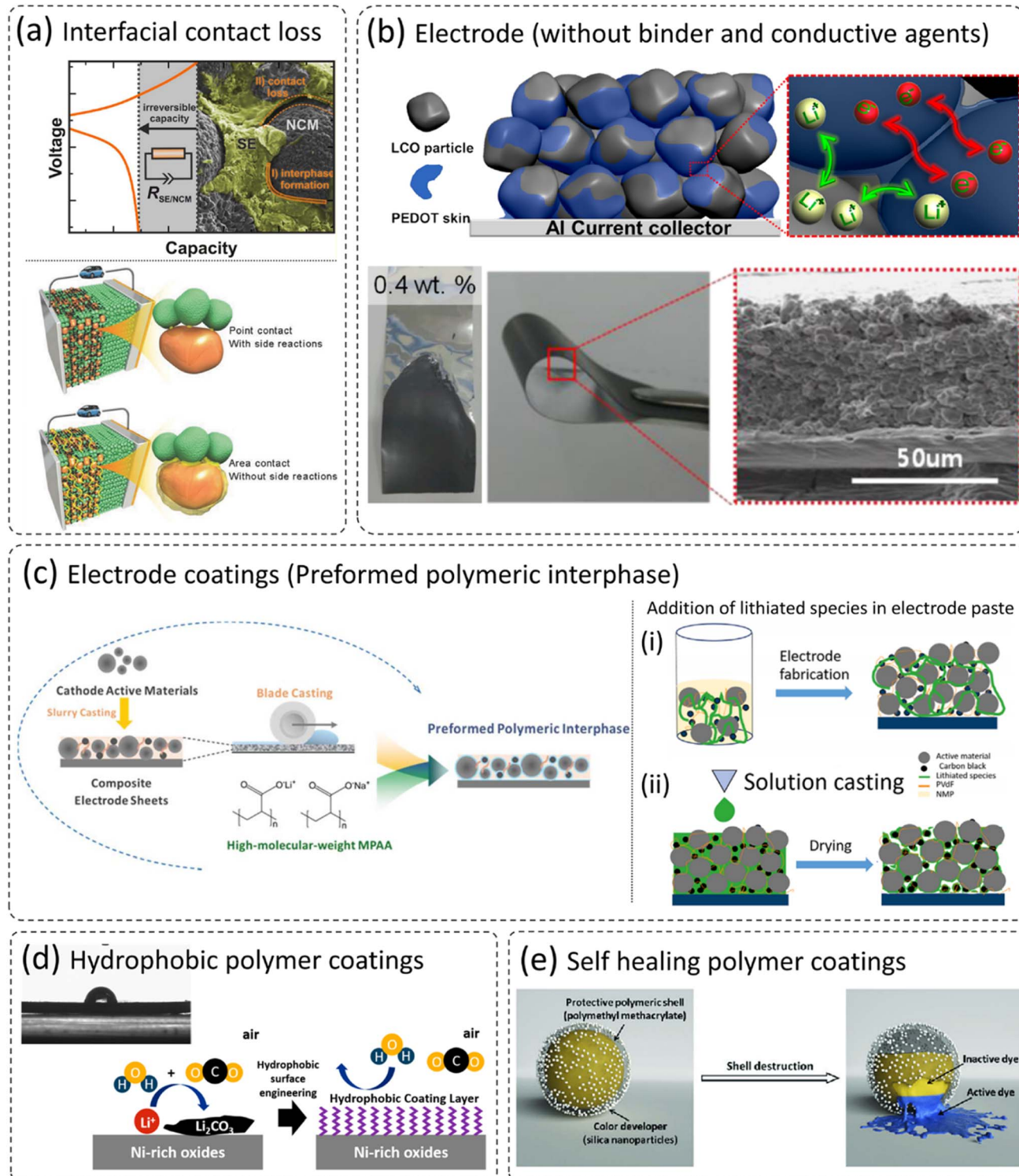


Fig. 8 (a) The problem of cathode/solid electrolyte interface delamination, and the beneficial role of polymer cathode coatings,<sup>120,143</sup> reproduced from ref. 120 with permission from American Chemical Society, copyright 2017, reproduced from ref. 143 with permission from Wiley, copyright 2018, (b) PEDOT coated LCO as a mono-component electrode (without additional conductive carbon and binder),<sup>121</sup> reproduced from ref. 121 with permission from American Chemical Society, copyright 2014, (c) possibility of polymer coatings on electrodes,<sup>22,24</sup> reproduced from ref. 22 with permission from The Electrochemical Society, copyright 2020, reproduced from ref. 24 with permission from The Royal Society of Chemistry, copyright 2018, (d) development of polymer-based hydrophobic cathode coatings, and (e) the concept of self-healing polymeric coatings, which may be translated to future cathode coatings,<sup>136</sup> reproduced from ref. 136 with permission from The Royal Society of Chemistry, copyright 2018.



performance of polymer coated electrodes was explained due to high ionic conductivities, the possibility of achieving thin conformal coatings, and good physical and chemical contact at the polymer coating/cathode surface.<sup>26,51,75-77,79-81,83-85,87-90</sup> A deeper insight was not sought in the literature. However, there might be a great possibility of *in situ* formation of an ultra-thin protective layer at the polymer and cathode interface during the coating development stage or in the formation cycle of the electrochemical cell. The newly formed protective layer might be stable at high voltage and enables the operation of the cell without further degradation and retains long-term cycling stability.

## 9. Applications of polymer coatings in ASSBs

It is well understood that cathode materials are prone to volume expansion/contraction during (de)lithiation. Therefore, during

successive cycling, cracks can form on the cathodes, which can lead to contact loss between cathode particles, and even with the current collector.<sup>41,55,116-119</sup> This effect is more pronounced in all-solid-state batteries (ASSBs) and leads to the loss of active cathodes, which results in capacity loss. In addition, the electrode and solid electrolyte can have contact loss due to volume expansion and contraction as shown in Fig. 8a,<sup>120</sup> and results in rapid irreversible capacity fade. Various strategies have been proposed to overcome the issues of cathode-solid electrolyte delamination in ASSBs such as (i) application of external pressure, (ii) addition of a small amount of liquid electrolyte, and (iii) application of ceramic-based coatings on the electrode surface. All these approaches are not cost-effective and not long-term sustainable. The addition of liquid electrolytes is not even in the line of ASSB definition. The incorporation of flexible polymer coatings can retain the contact between electrode particles and the cathode–electrolyte interface (Fig. 8a).

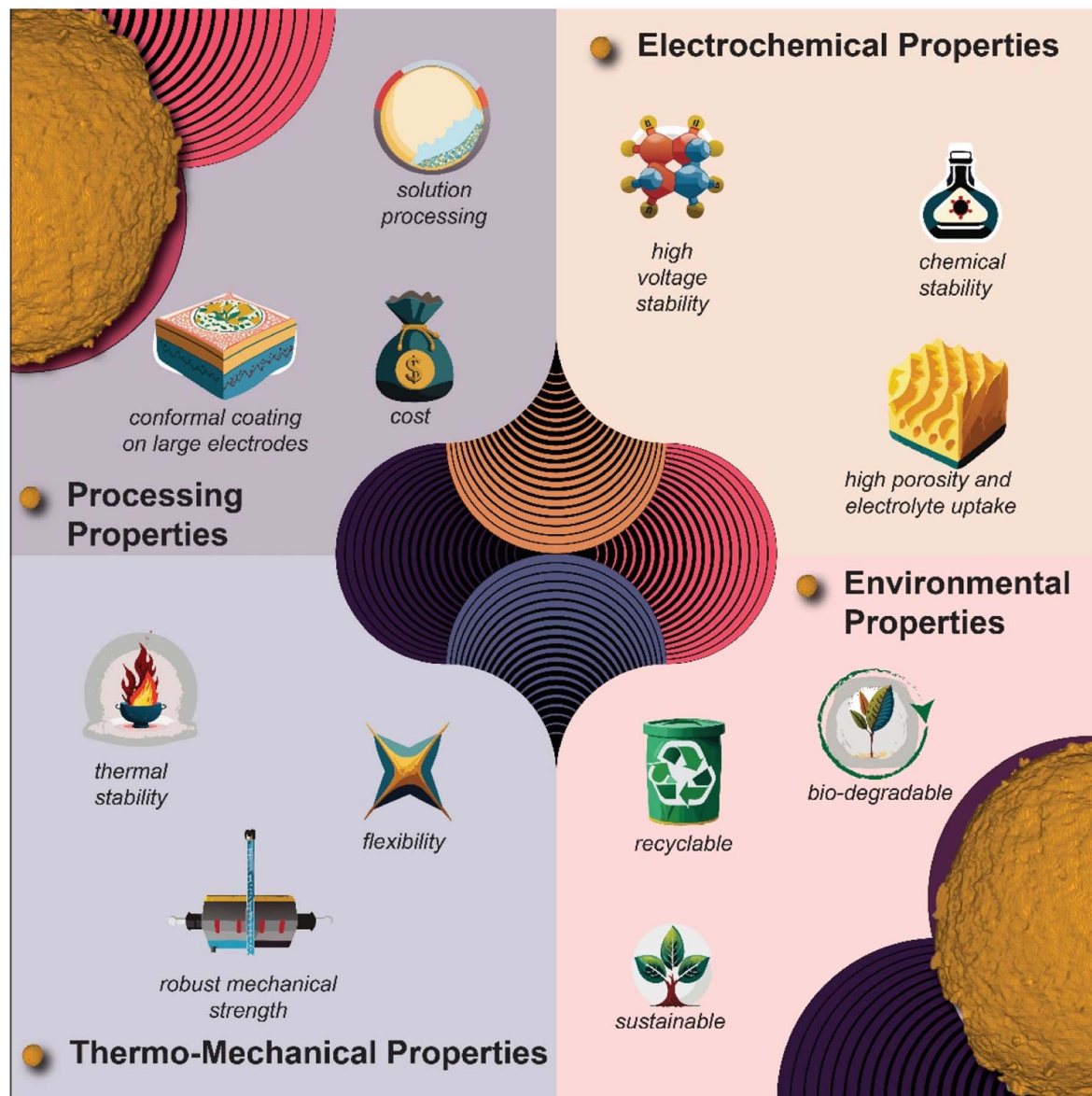


Fig. 9 Pictorial summary of polymer coating materials containing potential advantages over their inorganic counterpart.



However, the selection of polymer remains a challenge as it should be highly ionically conductive, has a wide electrochemical and chemical stability window, and prevents unwanted side reactions as already discussed in detail in the previous sections. Kim *et al.* developed a composite PEDOT:PSS coating on LiCoO<sub>2</sub> (LCO) cathodes and eliminated the use of additional binder and conductive agents for the fabrication of electrodes.<sup>121</sup> These mono-component electrodes can be employed in ASSBs and can potentially reduce non-electroactive components and enhance the energy density. The reported mono-component electrodes show both high ionic and electronic conductivity (PEDOT:PSS coated LCO in the absence of conductive carbon and PVDF binder). There was no significant physical breakage in the electrodes while bending as can be clearly seen in an SEM image in Fig. 8b.

Polymers have flexibility in terms of processing and experimental design and can be applied to electrode materials either before electrode fabrication or after fabrication.<sup>22,24,122</sup> Sun *et al.* applied a functional polyacrylate (PAA) based polymer coating on cast electrodes as shown in the schematic in Fig. 8c (ref. 24) and the coating thickness was estimated to be around 5 nm. This approach of polymer impregnation into an anode surface would be useful in solid-state batteries (SSBs). A similar approach of polymer impregnation using solution casting has been employed in SSBs as shown in the schematic in Fig. 8c (right side).<sup>22,123</sup> This concept of pore filling and thus ensuring good contact between cathode particles and solid electrolytes are very useful to realize its future application by forming an ionic and electronic conducting pathway.<sup>124–127</sup> The assembled solid-state battery exhibited low interfacial resistance, reduced cell polarization, and improved rate capability.<sup>123</sup> Moreover, the modified polymer can develop a hydrophobic coating to repel moisture and thus prevent the issues of surface instability and handling.<sup>111,112,128</sup> The approach can readily be helpful, especially in the case of (LiNi<sub>1-x-y</sub>Co<sub>x</sub>Mn<sub>y</sub>O<sub>2</sub>, Ni > 60%), which have poor ambient stability and are prone to undergo surface reactions with the residual lithium compounds (LiOH and Li<sub>2</sub>CO<sub>3</sub>).<sup>39,67,71,129–134</sup> Furthermore, the concept of self-healing polymer coatings is quite old in the field of corrosion protection of metallic components, especially in the oil and gas sector. These studies utilize similar concepts to prevent the exposure of fresh surfaces to electrolytes.<sup>135–142</sup> The intrinsically conductive polymers can repair defects and restore the protection of the substrate, restricting the potential chemical attack from the corrosive electrolyte. The temperature, pH, and mechanical stresses control the release of corrosion/healing inhibitor, which can be instigated in solid-state batteries for long-term cycling and high temperature/voltage operations. The presence of self-healing coatings on the electrode which can release self-healing agents to fill these gaps would be a breakthrough in ASSB technology, which can ultimately accelerate the commercialization of ASSBs.

## 10. Summary and future outlooks

This review article is focused comprehensively on the coating of high voltage cathode materials by using various types of

polymer materials and discussing their benefits, role, necessity, and suitability for ASSBs. The advantages and disadvantages of different polymers as a coating were elaborated in terms of improved interfacial properties and electrochemical performances. This article has extensively covered the comparison of the cycling performances of coated and uncoated high voltage cathodes under various operating conditions. It turned out that a polymer coating has the potential to improve battery performance. It revealed that the crystalline or amorphous morphology of the polymer coating does not have a significant impact on the electrochemical performance. However, the coating thickness plays an important role in the rate performance. An extremely thin coated (3–5 nm) layer has been developed using different coating strategies. The role of coatings in minimizing the detrimental structural change of cathodes in the charged state and side reactions was discussed briefly in the review.

It is not clearly understood why the cycling stability is greatly improved with polymer coatings in all cathode materials even, though most of the polymer materials are electrochemically unstable at a higher voltage. A deeper insight into the origin of stability was not sought in the literature. However, there might be a great possibility of *in situ* formation of an ultra-thin protective layer at the polymer and cathode interface at the coating development stage or in the formation cycle of the electrochemical cell. The newly formed protective layer might be stable at higher voltage and enables the operation of the cell without further degradation and retains long-term cycling stability. In ASSBs, the crack formation in the composite cathodes is more pronounced due to the volume expansion–contraction, which can lead to contact loss between cathode particles, the cathode/electrolyte interface, and even with the current collector. These effects lead to the loss of active materials, result in capacity loss, and generate cell overpotential. A polymer coating can minimize all these impacts due to its favorable mechanical properties and flexibility in terms of processing and experimental design.

Finally, the prospect of polymer-based surface coatings is evolving dynamically, offering remarkable flexibility as cathode coatings in Li-ion and ASSBs, as pictorially demonstrated in Fig. 9. Beyond the basic requirement of conformal surface coatings, the choice of polymer assumes paramount significance. Among the classes of polymers worthy of exploration for surface coating applications are ionic polymers, bio-based polymers, self-healing polymers, mixed-ionic electronic polymers, hydrophobic polymer coatings, redox polymers, and hybrid polymers (blending inorganic and polymer). Each type presents unique properties and advantages, contributing to the various options for tailored surface functionalities, and thus performance improvement.

## Conflicts of interest

The authors declare no competing financial interest.



## Acknowledgements

This research at the Oak Ridge National Laboratory, managed by UT Battelle, LLC, for the U.S. Department of Energy (DOE) under contract DE-AC05-00OR22725, was sponsored by the Laboratory Directed Research and Development (LDRD) Program at the Oak Ridge National Laboratory with project number 11060 and Office Electricity (OE) with project number 3CETE137.

## References

- 1 M. R. Palacín, *Chem. Soc. Rev.*, 2009, **38**, 2565–2575.
- 2 J.-M. Tarascon and M. Armand, *Nature*, 2001, **414**, 359–367.
- 3 Y. Huang, *Interdiscip. Mater.*, 2022, **1**, 323–329.
- 4 F. Cheng, J. Liang, Z. Tao and J. Chen, *Adv. Mater.*, 2011, **23**, 1695–1715.
- 5 A. Kraysberg and Y. Ein-Eli, *Adv. Energy Mater.*, 2012, **2**, 922–939.
- 6 J.-M. Tarascon, *Philos. Trans. R. Soc., A*, 2010, **368**, 3227–3241.
- 7 U. Nisar, R. Amin, R. Essehli, R. A. Shakoor, R. Kahraman, D. K. Kim, M. A. Khaleel and I. Belharouak, *J. Power Sources*, 2018, **396**, 774–781.
- 8 U. Nisar, R. Amin, A. Shakoor, R. Essehli, S. Al-Qaradawi, R. Kahraman and I. Belharouak, *Emergent Mater.*, 2018, **1**, 155–164.
- 9 P. Li, H. Kim, J. Ming, H. G. Jung, I. Belharouak and Y. K. Sun, *eScience*, 2021, **1**, 3–12.
- 10 D. D. MacNeil, Z. Lu, Z. Chen and J. R. Dahn, *J. Power Sources*, 2002, **108**, 8–14.
- 11 W.-S. Yoon, K.-W. Nam, D. Jang, K. Y. Chung, J. Hanson, J.-M. Chen and X.-Q. Yang, *J. Power Sources*, 2012, **217**, 128–134.
- 12 H. Konishi, M. Yoshikawa and T. Hirano, *J. Power Sources*, 2013, **244**, 23–28.
- 13 F. Chu, J. Hu, C. Wu, Z. Yao, J. Tian, Z. Li and C. Li, *ACS Appl. Mater. Interfaces*, 2019, **11**, 3869–3879.
- 14 C. H. Hu, Z. Q. Wang, Z. Y. Sun and C. Y. Ouyang, *Chem. Phys. Lett.*, 2014, **591**, 16–20.
- 15 F. Zhao, Q. Sun, C. Yu, S. Zhang, K. Adair, S. Wang, Y. Liu, Y. Zhao, J. Liang, C. Wang, X. Li, X. Li, W. Xia, R. Li, H. Huang, L. Zhang, S. Zhao, S. Lu and X. Sun, *ACS Energy Lett.*, 2020, **5**, 1035–1043.
- 16 H. Gao, N. S. Grundish, Y. Zhao, A. Zhou and J. B. Goodenough, *Energy Mater. Adv.*, 2021, **21**, 1932952.
- 17 J. Lau, R. H. DeBlock, D. M. Butts, D. S. Ashby, C. S. Choi and B. S. Dunn, *Adv. Energy Mater.*, 2018, **8**, 1800933.
- 18 Z.-Q. Wang, M. Wu, G. Liu, X. Lei, B. Xu and C. Ouyang, *Int. J. Electrochem. Sci.*, 2014, **9**, 562–568.
- 19 Z. Ning, D. S. Jolly, G. Li, R. De Meyere, S. D. Pu, Y. Chen, J. Kasemchainan, J. Ihli, C. Gong, B. Liu, D. L. R. Melvin, A. Bonnin, O. Magdysyuk, P. Adamson, G. O. Hartley, C. W. Monroe, T. J. Marrow and P. G. Bruce, *Nat. Mater.*, 2021, **20**, 1121–1129.
- 20 Z. Zhang, S. Chen, J. Yang, J. Wang, L. Yao, X. Yao, P. Cui and X. Xu, *ACS Appl. Mater. Interfaces*, 2018, **10**, 2556–2565.
- 21 H. Wan, G. Peng, X. Yao, J. Yang, P. Cui and X. Xu, *Energy Storage Mater.*, 2016, **4**, 59–65.
- 22 K. Borzutzki, M. Winter and G. Brunklaus, *J. Electrochem. Soc.*, 2020, **167**, 70546.
- 23 Q. Gan, N. Qin, Y. Zhu, Z. Huang, F. Zhang, S. Gu, J. Xie, K. Zhang, L. Lu and Z. Lu, *ACS Appl. Mater. Interfaces*, 2019, **11**, 12594–12604.
- 24 B. Sun, M. El Kazzi, E. Müller and E. J. Berg, *J. Mater. Chem. A*, 2018, **6**, 17778–17786.
- 25 D. Lu, Z. Yao, Y. Zhong, X. Wang, X. Xia, C. Gu, J. Wu and J. Tu, *ACS Appl. Mater. Interfaces*, 2019, **11**, 15630–15637.
- 26 G. L. Xu, Q. Liu, K. K. S. Lau, Y. Liu, X. Liu, H. Gao, X. Zhou, M. Zhuang, Y. Ren, J. Li, M. Shao, M. Ouyang, F. Pan, Z. Chen, K. Amine and G. Chen, *Nat. Energy*, 2019, **4**, 484–494.
- 27 U. Nisar, N. Muralidharan, R. Essehli, R. Amin and I. Belharouak, *Energy Storage Mater.*, 2021, **38**, 309–328.
- 28 U. Nisar, S. A. J. A. Al-Hail, R. K. Petla, R. A. Shakoor, R. Essehli, R. Kahraman, S. Y. AlQaradawi, D. K. Kim, I. Belharouak and M. R. Amin, *ACS Appl. Energy Mater.*, 2019, **2**, 7263–7271.
- 29 J. Song, X. Han, K. J. Gaskell, K. Xu, S. B. Lee and L. Hu, *J. Nanopart. Res.*, 2014, **16**, 1–8.
- 30 J. Liu and A. Manthiram, *J. Mater. Chem.*, 2010, **20**, 3961–3967.
- 31 H. Liu, Z. Zhang, Z. Gong and Y. Yang, *Solid State Ionics*, 2004, **166**, 317–325.
- 32 S. Hildebrand, C. Vollmer, M. Winter and F. M. Schappacher, *J. Electrochem. Soc.*, 2017, **164**, A2190–A2198.
- 33 Y. Cho, Y. S. Lee, S. A. Park, Y. Lee and J. Cho, *Electrochim. Acta*, 2010, **56**, 333–339.
- 34 D. Li, Y. Kato, K. Kobayakawa, H. Noguchi and Y. Sato, *J. Power Sources*, 2006, **160**, 1342–1348.
- 35 Q. Gan, N. Qin, Y. Zhu, Z. Huang, F. Zhang, S. Gu, J. Xie, K. Zhang, L. Lu and Z. Lu, *ACS Appl. Mater. Interfaces*, 2019, **11**, 12594–12604.
- 36 H. Kim, M. G. Kim, H. Y. Jeong, H. Nam and J. Cho, *Nano Lett.*, 2015, **15**, 2111–2119.
- 37 Y. Cho, P. Oh and J. Cho, *Nano Lett.*, 2013, **13**, 1145–1152.
- 38 Y. Cho, S. Lee, Y. Lee, T. Hong and J. Cho, *Adv. Energy Mater.*, 2011, **15**, 821–828.
- 39 B. Song, W. Li, P. Yan, S. M. Oh, C. M. Wang and A. Manthiram, *J. Power Sources*, 2016, **325**, 620–629.
- 40 C. Fu, G. Li, D. Luo, Q. Li, J. Fan and L. Li, *ACS Appl. Mater. Interfaces*, 2014, **6**, 15822–15831.
- 41 S.-T. Myung, H.-J. Noh, S.-J. Yoon, E.-J. Lee and Y.-K. Sun, *J. Phys. Chem. Lett.*, 2014, **5**, 671–679.
- 42 C. M. Julien, A. Mauger, H. Groult and K. Zaghib, *Thin Solid Films*, 2014, **572**, 200–207.
- 43 X. Lai, G. Hu, Z. Peng, H. Tong, Y. Lu, Y. Wang, X. Qi, Z. Xue, Y. Huang, K. Du and Y. Cao, *J. Power Sources*, 2019, **431**, 144–152.
- 44 M. C. Kim, S. H. Kim, V. Aravindan, W. S. Kim, S. Y. Lee and Y. S. Lee, *J. Electrochem. Soc.*, 2013, **160**, A1003–A1008.
- 45 Q. Xue, L. Li, Y. Huang, R. Huang, F. Wu and R. Chen, *ACS Appl. Mater. Interfaces*, 2019, **11**, 22339–22345.



46 F. Wu, J. Liu, L. Li, X. Zhang, R. Luo, Y. Ye and R. Chen, *ACS Appl. Mater. Interfaces*, 2016, **8**, 23095–23104.

47 T. Liu, M. Zhang, M. Zhu, Z. Du, W. Wang, Y. Wang, C. Xia and F. Chen, *J. Electrochem. Soc.*, 2020, **167**, 110510.

48 X. Jia, L. Wei, L. Xu, Y. Hu, H. Guo and Y. Li, *J. Alloys Compd.*, 2020, **832**, 154986.

49 Z. Liu, P. Hu, J. Ma, B. Qin, Z. Zhang, C. Mou, Y. Yao and G. Cui, *Electrochim. Acta*, 2017, **236**, 221–227.

50 J. Liu, F. Li, L. Xi, Z. Sun, Y. Yang, J. Shen, S. Yao, J. Zhao, M. Zhu and J. Liu, *Small*, 2024, **20**, e2305606.

51 H. Dong, Y. Zhang, S. Zhang, P. Tang, X. Xiao, M. Ma, H. Zhang, Y. Yin, D. Wang and S. Yang, *ACS Omega*, 2019, **4**, 185–194.

52 X. Lai, G. Hu, Z. Peng, H. Tong, Y. Lu, Y. Wang, X. Qi, Z. Xue, Y. Huang, K. Du and Y. Cao, *J. Power Sources*, 2019, 144–152.

53 L. Duan, J. Lu, W. Liu, P. Huang, W. Wang and Z. Liu, *Colloids Surf., A*, 2012, **414**, 98–103.

54 Y. Cho, S. Lee, Y. Lee, T. Hong and J. Cho, *Adv. Energy Mater.*, 2011, **1**, 821–828.

55 Z. Chen, Y. Qin and K. Amine, *J. Mater. Chem.*, 2010, **20**, 7606–7612.

56 D. Wang, X. Li, Z. Wang, H. Guo, Y. Xu, Y. Fan and J. Ru, *Electrochim. Acta*, 2016, **188**, 48–56.

57 U. Nisar, N. Muralidharan, R. Essehli, R. Amin and I. Belharouak, *Energy Storage Mater.*, 2021, **38**, 309–328.

58 U. Nisar, R. Petla, S. A. Jassim Al-Hail, A. A. Quddus, H. Monawwar, A. Shakoor, R. Essehli and R. Amin, *RSC Adv.*, 2020, **10**, 15274–15281.

59 U. Nisar, R. Amin, R. Essehli, R. A. Shakoor, R. Kahraman, D. K. Kim, M. A. Khaleel and I. Belharouak, *J. Power Sources*, 2018, **396**, 774–781.

60 Y. Liu, X. J. Lin, Y. G. Sun, Y. S. Xu, B. B. Chang, C. T. Liu, A. M. Cao and L. J. Wan, *Small*, 2019, **15**, 1–17.

61 H. Li and H. Zhou, *Chem. Commun.*, 2012, **48**, 1201.

62 J. Lu, C. Zhan, T. Wu, J. Wen, Y. Lei, A. J. Kropf, H. Wu, D. J. Miller, J. W. Elam, Y.-K. Sun, X. Qiu and K. Amine, *Nat. Commun.*, 2014, **5**, 5693.

63 H. Li, P. Zhou, F. Liu, H. Li, F. Cheng and J. Chen, *Chem. Sci.*, 2019, **10**, 1374–1379.

64 M. Iftekhar, N. E. Drewett, A. R. Armstrong, D. Hesp, F. Braga, S. Ahmed and L. J. Hardwick, *J. Electrochem. Soc.*, 2014, **161**, A2109–A2116.

65 J. Li, L. E. Downie, L. Ma, W. Qiu and J. R. Dahn, *J. Electrochem. Soc.*, 2015, **162**, A1401–A1408.

66 X. Li, L. Jin, D. Song, H. Zhang, X. Shi, Z. Wang, L. Zhang and L. Zhu, *J. Energy Chem.*, 2020, **40**, 39–45.

67 R. Hausbrand, G. Cherkashinin, H. Ehrenberg, M. Gr??ting, K. Albe, C. Hess and W. Jaegermann, *Materials Science and Engineering B: Solid State Materials for Advanced Technology*, 2015, **192**, 3–25.

68 J. Hu, Q. Wang, B. Wu, S. Tan, Z. Shadike, Y. Bi, M. S. Whittingham, J. Xiao, X. Q. Yang and E. Hu, *ACS Appl. Mater. Interfaces*, 2021, **13**, 2622–2629.

69 L. Co, M. O. Battery, Y. Lee, K. Nam, E. Hwang, Y. Kwon, D. Kang, S. Kim and S. Song, *J. Phys. Chem. C*, 2014, **118**, 10631–10639.

70 W. Liu, P. Oh, X. Liu, M. J. Lee, W. Cho, S. Chae, Y. Kim and J. Cho, *Angew. Chem., Int. Ed.*, 2015, **54**, 4440–4457.

71 Y.-K. Sun, B.-R. Lee, H.-J. Noh, H. Wu, S.-T. Myung and K. Amine, *J. Mater. Chem.*, 2011, **21**, 10108.

72 H. Konishi, T. Yuasa and M. Yoshikawa, *J. Power Sources*, 2011, **196**, 6884–6888.

73 H. Konishi, M. Yoshikawa and T. Hirano, *J. Power Sources*, 2013, **244**, 23–28.

74 L. Song, F. Tang, Z. Xiao, Z. Cao, H. Zhu and A. Li, *J. Electron. Mater.*, 2018, **47**, 5896–5904.

75 S. Y. Lee, J. H. Park, J. H. Cho, S. B. Kim, W. S. Kim and S. Y. Lee, *J. Mater. Chem.*, 2012, **22**, 12574–12581.

76 K. Kaliyappan, G. Li, L. Yang, Z. Bai and Z. Chen, *Energy Storage Mater.*, 2019, **22**, 168–178.

77 H. Q. Pham, G. Kim, H. M. Jung and S. W. Song, *Adv. Funct. Mater.*, 2018, **28**, 1–9.

78 J. Zhang, Q. Lu, J. Fang, J. Wang, J. Yang and Y. Nuli, *ACS Appl. Mater. Interfaces*, 2014, **6**, 17965–17973.

79 Q. Ran, H. Zhao, Y. Hu, Q. Shen, W. Liu, J. Liu, X. Shu, M. Zhang, S. Liu, M. Tan, H. Li and X. Liu, *Electrochim. Acta*, 2018, **289**, 82–93.

80 Z. Chen, K. Cao, H. Zhu, X. Gong, Q. Liu, J. Duan and L. Li, *Front. Chem.*, 2019, **7**, 1–10.

81 B. Li, G. Li, D. Zhang, J. Fan, D. Chen, Y. Ge, F. Lin, C. Zheng and L. Li, *ChemistrySelect*, 2019, **4**, 6354–6360.

82 X.-W. Gao, Y.-F. Deng, D. Wexler, G.-H. Chen, S.-L. Chou, H.-K. Liu, Z.-C. Shi and J.-Z. Wang, *J. Mater. Chem. A*, 2015, **3**, 404–411.

83 Y. Kwon, Y. Lee, S. O. Kim, H. S. Kim, K. J. Kim, D. Byun and W. Choi, *ACS Appl. Mater. Interfaces*, 2018, **10**, 29457–29466.

84 L. Su, P. M. Smith, P. Anand and B. Reeja-Jayan, *ACS Appl. Mater. Interfaces*, 2018, **10**, 27063–27073.

85 G. Hu, J. Fan, Y. Lu, Y. Zhang, K. Du, Z. Peng, L. Li, B. Zhang, Y. Shi and Y. Cao, *ChemSusChem*, 2020, **13**, 5699–5710.

86 Y. Huang, J. Xia, G. Hu, Y. Cao, Z. Peng, J. Fan, Y. Tao, T. Li, Z. Zhang, Z. Xue and K. Du, *Electrochim. Acta*, 2020, **332**, 135505.

87 Q. Zhang, J. Mei, X. Wang, F. Tang, W. Fan and W. Lu, *Electrochim. Acta*, 2014, **143**, 265–271.

88 X. Yang, L. Shen, B. Wu, Z. Zuo, D. Mu, B. Wu and H. Zhou, *J. Alloys Compd.*, 2015, **639**, 458–464.

89 H. Yan, W. Chen, X. Wu and Y. Li, *Electrochim. Acta*, 2014, **146**, 295–300.

90 Y. Cao, X. Qi, K. Hu, Y. Wang, Z. Gan, Y. Li, G. Hu, Z. Peng and K. Du, *ACS Appl. Mater. Interfaces*, 2018, **10**, 18270–18280.

91 J. Liu, Y. Chen, J. Xu, W. Sun, C. Zheng and Y. Li, *RSC Adv.*, 2019, **9**, 3081–3091.

92 M.-H. Choi, C. S. Yoon, S.-T. Myung, B.-B. Lim, S. Komaba and Y.-K. Sun, *J. Electrochem. Soc.*, 2015, **162**, A2313–A2318.

93 Y. K. Sun, M. J. Lee, C. S. Yoon, J. Hassoun, K. Amine and B. Scrosati, *Adv. Mater.*, 2012, **24**, 1192–1196.

94 T. Yoon, J. Soon, T. J. Lee, J. H. Ryu and S. M. Oh, *J. Power Sources*, 2021, **503**, 230051.

95 A. Manthiram, K. Chemelewski and E.-S. Lee, *Energy Environ. Sci.*, 2014, **7**, 1339.



96 H. Liu, R. Kloepsch, J. Wang, M. Winter and J. Li, *J. Power Sources*, 2015, **300**, 430–437.

97 T. Yi, J. Mei and Y. Zhu, *J. Power Sources*, 2016, **316**, 85–105.

98 J. H. Park, J. H. Cho, J. S. Kim, E. G. Shim and S. Y. Lee, *Electrochim. Acta*, 2012, **86**, 346–351.

99 J.-H. Cho, J.-H. Park, M.-H. Lee, H.-K. Song and S.-Y. Lee, *Energy Environ. Sci.*, 2012, **5**, 7124.

100 D. Becker, M. Börner, A. Friesen, S. Klein, U. Rodehorst, M. Diehl, M. Winter, T. Placke and R. Schmuck, *J. Electrochem. Soc.*, 2020, **167**, 060524.

101 T. Cheng, Z. Ma, R. Gu, R. Chen, Y. Lyu, A. Nie and B. Guo, *Energies*, 2018, **11**, 2712.

102 T. N. L. Doan, K. Yoo, T. K. a. Hoang and P. Chen, *Frontiers in Energy Research*, 2014, **2**, 1–7.

103 M. M. Thackeray, S.-H. Kang, C. S. Johnson, J. T. Vaughey, R. Benedek and S. a. Hackney, *J. Mater. Chem.*, 2007, **17**, 3112.

104 F. Wu, N. Li, Y. Su, L. Zhang, L. Bao, J. Wang, L. Chen, Y. Zheng, L. Dai, J. Peng and S. Chen, *Nano Lett.*, 2014, **14**, 3550–3555.

105 H. Shang, F. Ning, B. Li, Y. Zuo, S. Lu and D. Xia, *ACS Appl. Mater. Interfaces*, 2018, **10**, 21349–21355.

106 K. J. Rosina, M. Jiang, D. Zeng, E. Salager, A. S. Best and C. P. Grey, *J. Mater. Chem.*, 2012, **22**, 20605–20610.

107 T. Zhao, S. Chen, R. Chen, L. Li, X. Zhang, M. Xie and F. Wu, *ACS Appl. Mater. Interfaces*, 2014, **6**, 21711–21720.

108 L. Yao, F. Liang, J. Jin, B. V. R. Chowdari, J. Yang and Z. Wen, *Chem. Eng. J.*, 2020, **389**, 124403.

109 S. Chen, T. He, Y. Su, Y. Lu, L. Bao, L. Chen, Q. Zhang, J. Wang, R. Chen and F. Wu, *ACS Appl. Mater. Interfaces*, 2017, **9**, 29732–29743.

110 H. Yan, G. Zhang and Y. Li, *Appl. Surf. Sci.*, 2017, **393**, 30–36.

111 H. S. Kim, J. Kim, S. Kim, Y. D. Park and J. Mun, *Electrochim. Acta*, 2017, **246**, 51–58.

112 S. W. Doo, S. Lee, H. Kim, J. H. Choi and K. T. Lee, *ACS Appl. Energy Mater.*, 2019, **2**, 6246–6253.

113 S. E. Jerng, B. Chang, H. Shin, H. Kim, T. Lee, K. Char and J. W. Choi, *ACS Appl. Mater. Interfaces*, 2020, **12**, 10597–10606.

114 Z. X. Yang, R. G. Li and Z. H. Deng, *Sci. Rep.*, 2018, **8**, 4–11.

115 E. B. Chemere, F. M. Wang and W. C. Chien, *Surf. Coat. Technol.*, 2020, **398**, 126121.

116 S. H. Lee, C. S. Yoon, K. Amine and Y. K. Sun, *J. Power Sources*, 2013, **234**, 201–207.

117 A. Nurpeissova, M. H. Choi, J.-S. Kim, S.-T. Myung, S.-S. Kim and Y.-K. Sun, *J. Power Sources*, 2015, **299**, 425–433.

118 E. J. Lee, Z. Chen, H. J. Noh, S. C. Nam, S. Kang, D. H. Kim, K. Amine and Y. K. Sun, *Nano Lett.*, 2014, **14**, 4873–4880.

119 B. B. Lim, S. J. Yoon, K. J. Park, C. S. Yoon, S. J. Kim, J. J. Lee and Y. K. Sun, *Adv. Funct. Mater.*, 2015, **25**, 4673–4680.

120 R. Koever, I. Aygün, T. Leichtweiß, C. Dietrich, W. Zhang, J. O. Binder, P. Hartmann, W. G. Zeier and J. Janek, *Chem. Mater.*, 2017, **29**, 5574–5582.

121 J. M. Kim, H. S. Park, J. H. Park, T. H. Kim, H. K. Song and S. Y. Lee, *ACS Appl. Mater. Interfaces*, 2014, **6**, 12789–12797.

122 S. Kalluri, M. Yoon, M. Jo, H. K. Liu, S. X. Dou, J. Cho and Z. Guo, *Adv. Mater.*, 2017, **29**, 1605807.

123 S. Z. Zhang, X. H. Xia, D. Xie, R. C. Xu, Y. J. Xu, Y. Xia, J. B. Wu, Z. J. Yao, X. L. Wang and J. P. Tu, *J. Power Sources*, 2019, **409**, 31–37.

124 W. Cai, Y. Zhang, J. Li, Y. Sun and H. Cheng, *ChemSusChem*, 2014, **7**, 1063–1067.

125 C. Li, B. Qin, Y. Zhang, A. Varzi, S. Passerini, J. Wang, J. Dong, D. Zeng, Z. Liu and H. Cheng, *Adv. Energy Mater.*, 2019, **9**, 1803422.

126 C. Hänsel, E. Lizundia and D. Kundu, *ACS Appl. Energy Mater.*, 2019, **2**, 5686–5691.

127 Q. Pan, W. Zhang, M. Pan, B. Zhang, D. Zeng, Y. Sun and H. Cheng, *J. Power Sources*, 2015, **283**, 279–288.

128 Y. S. Wu, Q. T. Pham, C. C. Yang, C. S. Chern, L. Musuvadhi Babulal, M. Seenivasan, G. Brunklaus, T. Placke, B. J. Hwang and M. Winter, *Chem. Eng. J.*, 2021, **405**, 126727.

129 Y. Kim, H. Park, J. H. Warner and A. Manthiram, *ACS Energy Lett.*, 2021, **6**, 941–948.

130 A. Manthiram, J. C. Knight, S. T. Myung, S. M. Oh and Y. K. Sun, *Adv. Energy Mater.*, 2016, **6**, 1501010.

131 L. Wang, J. Li, X. He, W. Pu, C. Wan and C. Jiang, *J. Solid State Electrochem.*, 2009, **13**, 1157–1164.

132 D.-H. Cho, C.-H. Jo, W. Cho, Y.-J. Kim, H. Yashiro, Y.-K. Sun and S.-T. Myung, *J. Electrochem. Soc.*, 2014, **161**, A920–A926.

133 Y.-K. Sun, S.-T. Myung, B.-C. Park, J. Prakash, I. Belharouak and K. Amine, *Nat. Mater.*, 2009, **8**, 320–324.

134 J. Eom, M. G. Kim and J. Cho, *J. Electrochem. Soc.*, 2008, **155**, A239.

135 D. G. Shchukin, M. Zheludkevich, K. Yasakau, S. Lamaka, M. G. S. Ferreira and H. Möhwald, *Adv. Mater.*, 2006, **18**, 1672–1678.

136 M. Hu, S. Peil, Y. Xing, D. Döhler, L. Caire Da Silva, W. H. Binder, M. Kappl and M. B. Bannwarth, *Mater. Horiz.*, 2018, **5**, 51–58.

137 S. H. Cho, S. R. White and P. V. Braun, *Adv. Mater.*, 2009, **21**, 645–649.

138 S. Bode, L. Zedler, F. H. Schacher, B. Dietzek, M. Schmitt, J. Popp, M. D. Hager and U. S. Schubert, *Adv. Mater.*, 2013, **25**, 1634–1638.

139 D. G. Shchukin, *Polym. Chem.*, 2013, **4**, 4871–4877.

140 A. Yabuki, A. Kawashima and I. W. Fathona, *Corros. Sci.*, 2014, **85**, 141–146.

141 A. Yabuki, T. Shiraiwa and I. W. Fathona, *Corros. Sci.*, 2016, **103**, 117–123.

142 J. K. Wang, Q. Zhou, J. P. Wang, S. Yang and G. L. Li, *Colloids Surf. A*, 2019, **569**, 52–58.

143 L. P. Wang, X. D. Zhang, T. S. Wang, Y. X. Yin, J. L. Shi, C. R. Wang and Y. G. Guo, *Adv. Energy Mater.*, 2018, **8**, 1–8.

